

BROKEN-FEEC ON MULTIPATCH DOMAINS WITH LOCAL REFINEMENTS

FREDERIK SCHNACK AND MARTIN CAMPOS PINTO

ABSTRACT. This article introduces a novel approach for broken-FEEC (Finite Element Exterior Calculus), extending its application to locally refined spline spaces with non-matching interfaces. Traditional broken-FEEC allows for discontinuous discretizations at patch interfaces, preserving the de Rham structure and offering computational benefits. However, local refinements often lead to numerical artifacts. Our solution involves developing moment-preserving discrete conforming projection operators. These operators are explicit, localized, and metric-independent, ensuring H^1 and $H(\text{curl})$ continuity across non-matching interfaces while preserving high-order polynomial moments. This results in broken-FEEC de Rham sequences with accurate strong and weak derivatives, leading to energy-preserving Maxwell solvers that are explicit and virtually free of spurious modes. Numerical simulations confirm the efficacy of our method in eliminating spurious waves.

CONTENTS

1. Introduction	2
2. Broken-FEEC	4
2.1. Multipatch spline finite element spaces	4
2.2. Tensor-product and mapped spline bases	6
2.3. Conforming constraints on patch interfaces	7
2.4. Weak differential operators in conforming FEEC sequences	8
2.5. Weak broken differential operators and moment preservation	9
2.6. Broken-FEEC discretizations of model PDEs	11
3. Conforming projection operators on V_{pw}^0	15
3.1. Vertex-based projections	16
3.2. Edge-based projections	20
4. Conforming projection operators on V_{pw}^1	30
4.1. Edge-based projections	31
5. Numerical experiments	35
5.1. Approximation of the weak divergence	35
5.2. Poisson problem	37
5.3. Time-harmonic Maxwell problem	38
5.4. curl -curl eigenvalue problem	39
5.5. Time-domain Maxwell	40
5.6. Time-domain Helmholtz	42
6. Conclusion	42

2020 *Mathematics Subject Classification.* 65N30, 65N12, 65D07.

Key words and phrases. Commuting projection, finite element exterior calculus, de Rham sequence, multipatch spaces, isogeometric analysis.

References	42
Appendix A. Homogeneous boundary conditions	44
Appendix B. Implementation of conforming projections in practice	45
B.1. Correction coefficients γ	45
B.2. Matrix form of the extension- and restriction operators for V_{pw}^0	45
B.3. Matrix form of the extension- and restriction operators for V_{pw}^1	47

1. INTRODUCTION

Finite Element methods that preserve the de Rham structure underlying partial differential equations (PDEs) in electromagnetics and fluid dynamics have been extensively studied in the last decades [36, 33, 24, 4]. Following the pioneering works of Bossavit [8, 9] and Hiptmair [27, 28], the Hilbert complex analysis of Arnold, Falk and Winther [2, 3] has identified finite element exterior calculus (FEEC) as a unifying framework where the existence of bounded cochain projections is as driving force in the study of the intrinsic properties of these methods, such as the discrete stability, spectral accuracy and structure preservation previously established by other authors, see e.g. [1, 5, 7].

A powerful extension of these works has been developed in the context of isogeometric analysis methods [30], utilizing structure-preserving spline finite element spaces as proposed in [13]. These discretizations employ compatible sequences of tensor-product spline spaces, initially defined on a Cartesian parametric domain and then mapped to subdomains (referred to as patches) through pullback and push-forward operators. The parametric tensor-product structure is particularly advantageous, as it facilitates the implementation of efficient numerical algorithms while enabling the discretization of general domains with complex geometries. Other important contributions to multi-patch discretizations are the Mortar methods [11, 12]. In [26, 17] a *broken-FEEC* framework has been proposed for multi-patch spline spaces, following previous works on nonconforming versions of Nédélec's elements for Maxwell's equations [19]. In this framework, PDEs are discretized using finite element spaces which are fully discontinuous at the patch interfaces: local de Rham sequences are constructed on individual patches and strong differential operators are obtained by combining the single-patch (broken) derivatives with conforming projection operators which enforce the appropriate continuity conditions at the patch interfaces. An important point is that the underlying continuity is the minimal one to guarantee a Hilbert de Rham subcomplex property. In particular, no high order smoothness is required across patch interfaces, which allows the discrete conforming projections to be of geometric nature and metric independent. In turn, broken-FEEC discretizations have the attractive feature of preserving the de Rham structure and being equipped with local L^2 projection operators. Allowing discontinuities at the patch interfaces indeed leads to mass matrices which are block-diagonal, with blocks corresponding to individual patches. Inverse mass matrices are then also block-diagonal, which results in L^2 projections, Galerkin Hodge and discrete coderivatives being all local operators in the sense that their values on a given patch only depend on function values from that patch and its contiguous neighbors.

In this article, we address the issue of extending these constructions to locally refined spaces. A common scenario arises when adjacent patches are discretized using spline spaces of different resolutions, e.g. different knot sequences, resulting in non-matching interfaces as described in [16]. Such configurations allow for flexible handling of non-uniform smoothness and singularities in complex geometries, but they also pose several challenges. First, preserving the de Rham structure with locally refined splines remains an active area of research. Notable contributions include the construction of discrete de Rham sequences for T-splines and locally refined B-splines [15, 31], the study of exact sequences of hierarchical spline spaces [22], and the design of de Rham sequences for splines with varying degrees on domains with polar singularities [38, 34]. In [18], we analyzed the a priori stability of two-dimensional broken-FEEC discretizations with non-matching multipatch spaces, and showed that they admitted local bounded commuting projections under some connectivity conditions. A second challenge associated with local refinements is the appearance of numerical artifacts at non-matching patch interfaces. This issue is well-known in the context of wave propagation problems where spurious reflections have been observed on finite-difference grids with local refinements, and several interesting approaches have been devised to mitigate them. In [23] the authors study the good dispersion properties of an implicit “box” scheme, and its ability to avoid spurious modes on non-uniform grids. In [39] a numerical method is proposed that uses anisotropic perfectly matched layers to absorb spurious reflections around non-matching patch interfaces, and in [20, 21] the authors devise a fourth-order solver for Maxwell’s equations on locally refined Cartesian grids, that involves artificial damping and transition layers to mitigate the reflections.

In this article, we develop a structure-preserving alternative to these methods. Our approach is to equip broken-FEEC spaces with discrete conforming projection operators that preserve polynomial moments of arbitrary orders. In particular, we detail the construction of explicit projection matrices which enforce full and tangential continuity (corresponding to H^1 and $H(\text{curl})$ conformity, respectively) of the discrete fields across non-matching interfaces, while preserving integrals against high order polynomials on each logical patch. Our projection matrices are localized close to the patch interfaces and, like their basic low-order counterparts, they are metric independent. As a result, our broken-FEEC de Rham sequences have strong and weak (adjoint) derivatives which are both local and high-order accurate, leading to energy-preserving Maxwell solvers which are both explicit and asymptotically free of spurious modes.

The outline is as follows: in Section 2 we remind the main lines of the broken-FEEC framework and we illustrate it with discretizations of several model PDEs. A special attention is devoted to the description of weak differential operators associated with several types of boundary conditions, and to the importance of moment preservation in the underlying conforming projections operators. The construction of moment-preserving conforming projection operators on non-matching patch interfaces is then described in Section 3 and in Section 4, for H^1 and $H(\text{curl})$ - $H(\text{div})$ spaces respectively. Finally, numerical simulations are presented in Section 5. These experiments assess the properties of our numerical approach on the different discrete models previously described, and in particular they allow us to verify that spurious waves virtually disappear when moment-preserving projection matrices are used.

2. BROKEN-FEEC

In this article we consider finite element discretizations of the 2D grad-curl Rham sequence

$$(2.1) \quad V^0 = H^1(\Omega) \xrightarrow{\text{grad}} V^1 = H(\text{curl}; \Omega) \xrightarrow{\text{curl}} V^2 = L^2(\Omega)$$

defined on an open bounded domain $\Omega \subset \mathbb{R}^2$ with Lipschitz boundary, for which the adjoint sequence [2] is

$$(2.2) \quad L^2(\Omega) \xleftarrow{-\text{div}} H_0(\text{div}; \Omega) \xleftarrow{\text{curl}} H_0(\mathbf{curl} \Omega).$$

We will also address the sequence with homogeneous boundary conditions

$$(2.3) \quad V^0 = H_0^1(\Omega) \xrightarrow{\text{grad}} V^1 = H_0(\text{curl}; \Omega) \xrightarrow{\text{curl}} V^2 = L^2(\Omega)$$

for which the adjoint sequence is the inhomogeneous counterpart of (2.2).

We refer to [2, 3] for the analysis of these Hilbert complexes and their structure-preserving discretizations with finite element exterior calculus (FEEC) spaces. In this section we describe broken-FEEC spline spaces whose general properties have been studied in [26, 17], and we introduce the notation that will allow us to consider multipatch discretizations with nonuniform resolution. Notice that a strong discretization of (2.1) is naturally associated with a weak discretization of the adjoint sequence (2.2). By using a standard rotation argument, see e.g. [6, Rem. 2.3.2], one may also apply the constructions presented in this article to strong discretizations of the 2D curl-div sequences, namely

$$H(\mathbf{curl} \Omega) \xrightarrow{\text{curl}} H(\text{div}; \Omega) \xrightarrow{\text{div}} L^2(\Omega)$$

or its homogeneous counterpart (2.2).

An extension to the 3D de Rham sequence can also be derived by following the same approach, but is outside the scope of this article and will be addressed in a forthcoming work.

2.1. Multipatch spline finite element spaces. Our discretizations rely on spline finite element spaces associated with a multipatch domain, that is a domain of the form

$$\Omega = \text{int} \left(\bigcup_{k \in \mathcal{K}} \overline{\Omega_k} \right) \quad \text{with} \quad \Omega_k = F_k(\hat{\Omega}),$$

with disjoint, geometrically conforming subdomains Ω_k parametrized by smooth (C^1 diffeomorphism) mappings F_k with patch indices $k \in \mathcal{K} = \{1, \dots, K\}$, and a reference Cartesian domain $\hat{\Omega} =]0, 1[^2$.

Following [14, 13], on the mapped subdomains we consider mapped spline spaces obtained by pushing forward logical tensor-product splines. For each patch k we then first consider two univariate spline spaces on the interval $[0, 1]$ forming a 1D de Rham sequence,

$$(2.4) \quad \mathbb{V}_k^0 := \mathbb{S}^p[\Xi_k], \quad \xrightarrow{\partial_{\hat{x}}} \quad \mathbb{V}_k^1 := \mathbb{S}^{p-1}[\Xi'_k].$$

These spaces consist of clamped splines of respective degree p and $p-1$, defined by two knot vectors $\Xi_k = (\xi_i^k)_{i=0}^{n_k+1+p}$ and $(\Xi_k)' = (\xi_i^k)_{i=1}^{n_k+p}$, associated with knots of the form

$$(2.5) \quad 0 = \xi_0 = \dots = \xi_p < \xi_{p+1} < \dots < \xi_{n_k+1} = \dots = \xi_{n_k+1+p} = 1.$$

Here $n_k = \dim(\mathbb{V}_k^1) = \dim(\mathbb{V}_k^0) - 1$, and we refer to, e.g., [37] for a detailed description of univariate spline spaces and B-spline bases. The knots (2.5) define the resolution in the patch k , which is allowed to vary from that of the other patches under a nestedness assumption that will be specified below. A de Rham sequence on the logical domain $\hat{\Omega}$ is then obtained by considering the tensor-product spaces

$$\hat{V}_k^0 := \mathbb{V}_k^0 \otimes \mathbb{V}_k^0 \xrightarrow{\mathbf{grad}} \hat{V}_k^1 := \begin{pmatrix} \mathbb{V}_k^1 \otimes \mathbb{V}_k^0 \\ \mathbb{V}_k^0 \otimes \mathbb{V}_k^1 \end{pmatrix} \xrightarrow{\mathbf{curl}} \hat{V}_k^2 := \mathbb{V}_k^1 \otimes \mathbb{V}_k^1,$$

and on the mapped patch $\Omega_k = F_k(\hat{\Omega})$ we consider the spaces

$$(2.6) \quad V_k^0 := \mathcal{F}_k^0(\hat{V}_k^0) \xrightarrow{\mathbf{grad}} V_k^1 := \mathcal{F}_k^1(\hat{V}_k^1) \xrightarrow{\mathbf{curl}} V_k^2 := \mathcal{F}_k^2(\hat{V}_k^2)$$

associated with the pushforward operators associated with F_k . In 2D, they read

$$\begin{cases} \mathcal{F}_k^0 : \hat{\phi} \mapsto \phi := \hat{\phi} \circ F_k^{-1} \\ \mathcal{F}_k^1 : \hat{\mathbf{u}} \mapsto \mathbf{u} := (DF_k^{-T} \hat{\mathbf{u}}) \circ F_k^{-1} \\ \mathcal{F}_k^2 : \hat{f} \mapsto f := (J_{F_k}^{-1} \hat{f}) \circ F_k^{-1} \end{cases}$$

where $DF_k(\hat{x}) = (\partial_b(F_k)_a(\hat{x}))_{1 \leq a, b \leq 2}$ is the Jacobian matrix of F_k , and J_{F_k} its metric determinant, see e.g. [28, 32, 10, 29].

The broken-FEEC discretization then involves two sequences of spaces for the global domain Ω : a sequence of broken spaces which are fully discontinuous at the patch interfaces, hence only *patch-wise smooth*,

$$(2.7) \quad V_{\text{pw}}^\ell := \{v \in L^2(\Omega) : v|_{\Omega_k} \in V_k^\ell \text{ for } k \in \mathcal{K}\}, \quad \ell \in \{0, 1, 2\}$$

and a sequence of conforming subspaces

$$(2.8) \quad V_h^\ell := V_{\text{pw}}^\ell \cap V^\ell = \{v \in V^\ell : v|_{\Omega_k} \in V_k^\ell \text{ for } k \in \mathcal{K}\}.$$

As a result of the global de Rham sequence structure (2.1) or (2.3), and of that of the local ones (2.6) which follow from the commutation properties of the pushforward operators [28], the conforming spaces also form a de Rham sequence,

$$V_h^0 \xrightarrow{\mathbf{grad}} V_h^1 \xrightarrow{\mathbf{curl}} V_h^2.$$

Its stability and structure-preserving properties have been analyzed in [18], where L^2 stable commuting projection operators have been constructed under some connectivity conditions, yielding a commuting diagram for multi-patch spaces with non-matching interfaces:

$$\begin{array}{ccccc} V^0 & \xrightarrow{\mathbf{grad}} & V^1 & \xrightarrow{\mathbf{curl}} & V^2 \\ \downarrow \Pi^0 & & \downarrow \Pi^1 & & \downarrow \Pi^2 \\ V_h^0 & \xrightarrow{\mathbf{grad}} & V_h^1 & \xrightarrow{\mathbf{curl}} & V_h^2. \end{array}$$

Broken-FEEC schemes rely on *conforming projection operators*

$$(2.9) \quad P^\ell : V_{\text{pw}}^\ell \rightarrow V_h^\ell \subset V_{\text{pw}}^\ell$$

whose primary purpose is to enforce the relevant continuity conditions at the patch interfaces. These discrete projections endow the broken spaces (2.7) with a discrete de Rham structure

$$V_{\text{pw}}^0 \xrightarrow{\mathbf{grad} P^0} V_{\text{pw}}^1 \xrightarrow{\mathbf{curl} P^1} V_{\text{pw}}^2$$

and an adjoint discrete sequence may be defined by L^2 duality,

$$(2.10) \quad V_{\text{pw}}^0 \xleftarrow{(\mathbf{grad} P^0)^*} V_{\text{pw}}^1 \xleftarrow{(\mathbf{curl} P^1)^*} V_{\text{pw}}^2.$$

A key observation is that (2.10) can only be a high-order discretization of the continuous sequence (2.2) if the adjoint conforming projections $(P^\ell)^*$ are high-order accurate. That is, if the projections (2.9) preserve high order polynomial moments. Their construction on non-matching multipatch spline spaces will be the main goal of this work.

2.2. Tensor-product and mapped spline bases. The univariate spaces (2.4) can be classically equipped with B-spline basis functions,

$$(2.11) \quad \mathbb{V}_k^0 = \text{Span}(\{\lambda_i^{0,k} : i = 0, \dots, n_k\}), \quad \mathbb{V}_k^1 = \text{Span}(\{\lambda_i^{1,k} : i = 0, \dots, n_k - 1\}).$$

Since we will mostly use the former ones to define our projection operators, we drop the space index for conciseness and write

$$\lambda_i^k := \lambda_i^{0,k}, \quad 0 \leq i \leq n_k.$$

From the form of the open knot vector (2.5), it follows that these functions satisfy an interpolation property at the endpoints, namely

$$\lambda_i^k(0) = \delta_{i,0} \quad \text{and} \quad \lambda_i^k(1) = \delta_{i,n_k}.$$

Moreover the underlying patch grid has $N_k = n_k + 1 - p$ cells in each direction. For later purposes we assume a minimal resolution for the patches.

Assumption 2.1. The number of cells per dimension satisfies $N_k \geq 3$ for all $k \in \mathcal{K}$.

The bivariate basis functions on the logical domain $\hat{\Omega}$ are then defined as tensor products: for \hat{V}_k^0 we set

$$(2.12) \quad \hat{\Lambda}_{\mathbf{i}}^k(\hat{\mathbf{x}}) := \lambda_{i_1}^k(\hat{x}_1) \lambda_{i_2}^k(\hat{x}_2) \quad \text{for } \mathbf{i} = (i_1, i_2) \in \mathcal{I}^k := \{0, \dots, n_k\}^2,$$

for the space \hat{V}_k^1 we have

$$\begin{cases} \hat{\Lambda}_{1,\mathbf{i}}^{1,k}(\hat{\mathbf{x}}) := \begin{pmatrix} \lambda_{i_1}^{1,k}(\hat{x}_1) \lambda_{i_2}^k(\hat{x}_2) \\ 0 \end{pmatrix} & \text{for } \mathbf{i} \in \mathcal{I}_1^{1,k} := \{0, \dots, n_k - 1\} \times \{0, \dots, n_k\}, \\ \hat{\Lambda}_{2,\mathbf{i}}^{1,k}(\hat{\mathbf{x}}) := \begin{pmatrix} 0 \\ \lambda_{i_1}^k(\hat{x}_1) \lambda_{i_2}^{1,k}(\hat{x}_2) \end{pmatrix} & \text{for } \mathbf{i} \in \mathcal{I}_2^{1,k} := \{0, \dots, n_k\} \times \{0, \dots, n_k - 1\}, \end{cases}$$

and for conciseness we set $\mathcal{I}^{1,k} := \{(d, \mathbf{i}) : d \in \{1, 2\}, \mathbf{i} \in \mathcal{I}_d^{1,k}\}$. Finally for \hat{V}_k^2 we set

$$\hat{\Lambda}_{\mathbf{i}}^{2,k}(\hat{\mathbf{x}}) := \lambda_{i_1}^{1,k}(\hat{x}_1) \lambda_{i_2}^{1,k}(\hat{x}_2) \quad \text{for } \mathbf{i} \in \mathcal{I}^{2,k} := \{0, \dots, n_k - 1\}^2.$$

Finally the basis functions for the broken spaces (2.7) are obtained by pushing forward the reference basis functions on the mapped patches Ω_k , $k \in \mathcal{K}$, and extending them by zero outside of their patch. The basis of V_{pw}^0 thus reads

$$(2.13) \quad \Lambda_{\mathbf{i}}^k(\mathbf{x}) := \mathcal{F}_k^0(\hat{\Lambda}_{\mathbf{i}}^k)(\mathbf{x}) = \begin{cases} \hat{\Lambda}_{\mathbf{i}}^k(\hat{\mathbf{x}}^k) & \text{on } \Omega_k \\ 0 & \text{elsewhere} \end{cases} \quad \text{for } k \in \mathcal{K}, \quad \mathbf{i} \in \mathcal{I}^k$$

where we have written $\hat{\mathbf{x}}^k := (F_k)^{-1}(\mathbf{x})$. Similarly, the basis of V_{pw}^1 reads

$$\Lambda_{d,i}^{1,k}(\mathbf{x}) := \mathcal{F}_k^1(\hat{\Lambda}_{d,i}^{1,k})(\mathbf{x}) = \begin{cases} DF_k^{-T} \hat{\Lambda}_{d,i}^{1,k}(\hat{\mathbf{x}}^k) & \text{on } \Omega_k \\ 0 & \text{elsewhere} \end{cases} \quad \text{for } k \in \mathcal{K}, (d,i) \in \mathcal{I}^{1,k}$$

and the basis of V_{pw}^2 reads

$$\Lambda_i^{2,k}(\mathbf{x}) := \mathcal{F}_k^2(\hat{\Lambda}_i^{2,k})(\mathbf{x}) = \begin{cases} J_k^{-1} \hat{\Lambda}_i^{2,k}(\hat{\mathbf{x}}^k) & \text{on } \Omega_k \\ 0 & \text{elsewhere} \end{cases} \quad \text{for } k \in \mathcal{K}, i \in \mathcal{I}^{2,k}.$$

2.3. Conforming constraints on patch interfaces. Since the local spaces V_k^ℓ consist of continuous functions, the conforming subspaces $V_h^\ell \subset V_{\text{pw}}^\ell$ may be characterized by continuity constraints on the patch interfaces, namely on the intersections of patch boundaries $\partial\Omega_k \cap \partial\Omega_l$, $k \neq l$. Because we assume that patches are geometrically conforming, these interfaces are either an edge or a vertex of both patches, and it follows from the Lipschitz assumption on $\partial\Omega$ that if a vertex is shared by two patches, then it belongs to an edge also shared by two patches (an interior edge). In particular, the continuity constraints characterizing the conforming spaces (2.8) may be expressed on interior edges.

For the first space $V_h^0 = V_{\text{pw}}^0 \cap V^0$, with $V^0 = H^1(\Omega)$ as in (2.1), the continuity condition reads: $\phi \in V_{\text{pw}}^0$ belongs to V^0 if and only if

$$\phi|_{\Omega_{k-}} = \phi|_{\Omega_{k+}} \quad \text{on every interior edge } e = \partial\Omega_{k-} \cap \partial\Omega_{k+}.$$

In the case of homogeneous boundary conditions (2.3) where $V^0 = H_0^1(\Omega)$, an additional condition is imposed on the boundary edges, namely

$$\phi|_e = 0 \quad \text{on every boundary edge } e \subset \partial\Omega.$$

Similarly, a function $\mathbf{u} \in V_{\text{pw}}^1$ belongs to $V^1 = H(\text{curl}; \Omega)$ if and only if

$$\boldsymbol{\tau} \cdot \mathbf{u}|_{\Omega_{k-}} = \boldsymbol{\tau} \cdot \mathbf{u}|_{\Omega_{k+}} \quad \text{on every interior edge } e = \partial\Omega_{k-} \cap \partial\Omega_{k+}$$

where $\boldsymbol{\tau}$ denotes an arbitrary vector tangent to the edge. For the sequence (2.1) this characterizes the vector fields in V_h^1 . In the case of homogeneous boundary conditions (2.3) where $V^1 = H_0(\text{curl}; \Omega)$, an additional condition is imposed on the boundary edges, namely

$$\boldsymbol{\tau} \cdot \mathbf{u}|_e = 0 \quad \text{on every boundary edge } e \subset \partial\Omega.$$

For the last space of the sequence there are no constraints: since $V^2 = L^2(\Omega)$, the conforming space is simply $V_h^2 = V_{\text{pw}}^2$.

For later purposes we denote by \mathcal{E} and \mathcal{V} the respective sets of patch edges and vertices. Given $e \in \mathcal{E}$, we gather the indices of adjacent patches in

$$\mathcal{K}(e) = \{k \in \mathcal{K} : e \subset \partial\Omega_k\},$$

and similarly for a given $v \in \mathcal{V}$, we gather the indices of the adjacent patches in the set

$$\mathcal{K}(v) = \{k \in \mathcal{K} : v \in \partial\Omega_k\}.$$

We also define patch neighborhoods of edges and vertices as

$$\Omega(e) := \text{int} \left(\bigcup_{k \in \mathcal{K}(e)} \overline{\Omega_k} \right), \quad \Omega(v) := \text{int} \left(\bigcup_{k \in \mathcal{K}(v)} \overline{\Omega_k} \right).$$

Clearly, $\mathcal{K}(e)$ contains two patches if e is an interior edge, and only one patch if it is a boundary edge.

Assumption 2.2. Interior edges e are shared by two patches of nested resolutions, in the sense that $\mathcal{K}(e)$ is of the form $\{k^-(e), k^+(e)\}$ with

$$\mathbb{V}_{k^-(e)}^0 \subset \mathbb{V}_{k^+(e)}^0.$$

2.4. Weak differential operators in conforming FEEC sequences. In this section and the following one, we specify in which sense discrete adjoint sequences such as (2.10) approximate the continuous ones. Our main observation will be that broken-FEEC spaces allow more flexibility than conforming ones in the choice of the underlying weak boundary conditions. We will also specify a notion of moment preservation that will allow us to reach high-order accuracy for the weak differential operators.

Let us begin by reminding that if one considers the grad-curl sequence *without* boundary conditions (2.1) as a primal de Rham sequence, then the associated adjoint sequence, defined by L^2 duality, is the curl-div sequence *with* homogeneous boundary conditions (2.2). Conversely, if the grad-curl sequence with boundary conditions (2.3) is chosen as a primal de Rham sequence, then the corresponding adjoint sequence is the curl-div sequence without boundary conditions.

At the discrete level a similar behavior can be observed. For instance in the case of conforming spaces V_h^ℓ approximating the inhomogeneous sequence (2.1), one may expect that the discrete adjoint operators approximate the continuous differential operators with homogeneous boundary conditions. This can be verified by considering $\text{div}_{h,0} := -(\mathbf{grad})^* : V_h^1 \rightarrow V_h^0$ and $\mathbf{curl}_{h,0} := (\mathbf{curl})^* : V_h^2 \rightarrow V_h^1$ defined by the relations

$$(2.14) \quad \begin{cases} \langle \phi, \text{div}_{h,0} \mathbf{u} \rangle = -\langle \mathbf{grad} \phi, \mathbf{u} \rangle, & \forall \mathbf{u} \in V_h^1, \phi \in V_h^0, \\ \langle \mathbf{v}, \mathbf{curl}_{h,0} w \rangle = \langle \mathbf{curl} \mathbf{v}, w \rangle, & \forall w \in V_h^2, \mathbf{v} \in V_h^1, \end{cases}$$

and letting $\tilde{\Pi}_h^\ell$ be the L^2 projection onto V_h^ℓ . Then, the following relations hold:

$$\begin{cases} \text{div}_{h,0} \tilde{\Pi}_h^1 \mathbf{u} = \tilde{\Pi}_h^0 \text{div} \mathbf{u}, & \forall \mathbf{u} \in H_0(\text{div}; \Omega), \\ \mathbf{curl}_{h,0} \tilde{\Pi}_h^2 \mathbf{v} = \tilde{\Pi}_h^1 \mathbf{curl} \mathbf{v}, & \forall \mathbf{v} \in H_0(\mathbf{curl}; \Omega). \end{cases}$$

Indeed, for all $\phi \in V_h^0$ and $\mathbf{u} \in H_0(\text{div}; \Omega)$ we have

$$\langle \phi, \text{div}_{h,0} \tilde{\Pi}_h^1 \mathbf{u} \rangle = -\langle \mathbf{grad} \phi, \tilde{\Pi}_h^1 \mathbf{u} \rangle = -\langle \mathbf{grad} \phi, \mathbf{u} \rangle = \langle \phi, \text{div} \mathbf{u} \rangle = \langle \phi, \tilde{\Pi}_h^0 \text{div} \mathbf{u} \rangle,$$

and the relation involving $\mathbf{curl}_{h,0}$ is verified in the same way.

Conversely, if the conforming spaces (denoted here $V_{h,0}^\ell$ for clarity) approximate the sequence (2.3) *with* homogeneous boundary conditions, then the discrete adjoint operators approximate the continuous differential operators *without* boundary conditions. To specify this, consider the operators $\text{div}_h := -(\mathbf{grad})^* : V_{h,0}^1 \rightarrow V_{h,0}^0$ and $\mathbf{curl}_h := (\mathbf{curl})^* : V_{h,0}^2 \rightarrow V_{h,0}^1$ defined by the relations

$$(2.15) \quad \begin{cases} \langle \phi, \text{div}_h \mathbf{u} \rangle = -\langle \mathbf{grad} \phi, \mathbf{u} \rangle, & \forall \mathbf{u} \in V_{h,0}^1, \phi \in V_{h,0}^0, \\ \langle \mathbf{v}, \mathbf{curl}_h w \rangle = \langle \mathbf{curl} \mathbf{v}, w \rangle, & \forall w \in V_{h,0}^2, \mathbf{v} \in V_{h,0}^1, \end{cases}$$

and let $\tilde{\Pi}_{h,0}^\ell$ be the L^2 projection onto $V_{h,0}^\ell$. Then the following relations hold:

$$\begin{cases} \text{div}_h \tilde{\Pi}_{h,0}^1 \mathbf{u} = \tilde{\Pi}_{h,0}^0 \text{div} \mathbf{u}, & \forall \mathbf{u} \in H(\text{div}; \Omega), \\ \mathbf{curl}_h \tilde{\Pi}_{h,0}^2 \mathbf{v} = \tilde{\Pi}_{h,0}^1 \mathbf{curl} \mathbf{v}, & \forall \mathbf{v} \in H(\mathbf{curl}; \Omega). \end{cases}$$

Again, this is easy to establish: for all $\phi \in V_{h,0}^0$ and $\mathbf{u} \in H(\text{div}; \Omega)$, compute

$$\langle \phi, \text{div}_h \tilde{\Pi}_{h,0}^1 \mathbf{u} \rangle = -\langle \mathbf{grad} \phi, \tilde{\Pi}_{h,0}^1 \mathbf{u} \rangle = -\langle \mathbf{grad} \phi, \mathbf{u} \rangle = \langle \phi, \text{div} \mathbf{u} \rangle = \langle \phi, \tilde{\Pi}_{h,0}^0 \text{div} \mathbf{u} \rangle,$$

and the relation involving \mathbf{curl}_h is verified in the same way. We may summarize these observations as follows.

Theorem 2.3. *Let $\tilde{\Pi}_h^\ell$ be the L^2 -projection onto the conforming space V_h^ℓ without boundary conditions, and let*

$$\text{div}_{h,0} := -(\mathbf{grad})^* : V_h^1 \rightarrow V_h^0, \quad \mathbf{curl}_{h,0} := (\mathbf{curl})^* : V_h^2 \rightarrow V_h^1$$

be the discrete differential operators corresponding to (2.14). Then the following diagram commutes:

$$\begin{array}{ccccc} V_h^0 & \xrightleftharpoons[\text{div}_{h,0}]{\mathbf{grad}} & V_h^1 & \xrightleftharpoons[\mathbf{curl}_{h,0}]{\mathbf{curl}} & V_h^2 \\ \tilde{\Pi}_h^0 \uparrow & & \tilde{\Pi}_h^1 \uparrow & & \tilde{\Pi}_h^2 \uparrow \\ L^2 & \xleftarrow{\text{div}} & H_0(\text{div}) & \xleftarrow{\mathbf{curl}} & H_0(\mathbf{curl}) \end{array}$$

Conversely, let $\tilde{\Pi}_{h,0}^\ell$ be the L^2 -projection onto the conforming space with homogeneous boundary conditions $V_{h,0}^\ell$, and let

$$\text{div}_h := -(\mathbf{grad})^* : V_{h,0}^1 \rightarrow V_{h,0}^0, \quad \mathbf{curl}_h := (\mathbf{curl})^* : V_{h,0}^2 \rightarrow V_{h,0}^1$$

be the discrete differential operators corresponding to (2.15). Then the following diagram commutes:

$$\begin{array}{ccccc} V_{h,0}^0 & \xrightleftharpoons[\text{div}_h]{\mathbf{grad}_0} & V_{h,0}^1 & \xrightleftharpoons[\mathbf{curl}_h]{\mathbf{curl}_0} & V_{h,0}^2 \\ \tilde{\Pi}_{h,0}^0 \uparrow & & \tilde{\Pi}_{h,0}^1 \uparrow & & \tilde{\Pi}_{h,0}^2 \uparrow \\ L^2 & \xleftarrow{\text{div}} & H(\text{div}) & \xleftarrow{\mathbf{curl}} & H(\mathbf{curl}) \end{array}$$

In particular, the boundary conditions associated with the weak differential operators are determined by the underlying conforming finite element spaces.

2.5. Weak broken differential operators and moment preservation. In the broken-FEEC framework, boundary conditions are not imposed on the finite element spaces themselves (which are defined patch-wise without taking into account neighboring patches or global constraints) but through the conforming projection operators. As a result, one can expect that the above duality principle applies in a flexible way, allowing one to choose the weak boundary conditions by selecting a suitable conforming projection. To verify this flexible duality principle, let us assume that

$$P^\ell : V_{\text{pw}}^\ell \rightarrow V_h^\ell \quad \text{and} \quad P_0^\ell : V_{\text{pw}}^\ell \rightarrow V_{h,0}^\ell$$

are conforming projection operators onto the discrete spaces without and with homogeneous boundary conditions, respectively. Examples of such projections will be described later in this article. We may then consider two kinds of weak differential operators, as above. First, the adjoints of the strong broken-FEEC differential operators associated with *no* boundary conditions, which should in principle approximate the adjoint differential operators *with* homogeneous boundary conditions:

$\text{div}_{\text{pw},0} := -(\mathbf{grad} P^0)^* : V_{\text{pw}}^1 \rightarrow V_{\text{pw}}^0$ and $\mathbf{curl}_{\text{pw},0} := (\text{curl} P^1)^* : V_{\text{pw}}^2 \rightarrow V_{\text{pw}}^1$, defined by the relations

$$(2.16) \quad \begin{cases} \langle \phi, \text{div}_{\text{pw},0} \mathbf{u} \rangle = -\langle \mathbf{grad} P^0 \phi, \mathbf{u} \rangle, & \forall \mathbf{u} \in V_{\text{pw}}^1, \phi \in V_{\text{pw}}^0, \\ \langle \mathbf{v}, \mathbf{curl}_{\text{pw},0} w \rangle = \langle \text{curl} P^1 \mathbf{v}, w \rangle, & \forall w \in V_{\text{pw}}^2, \mathbf{v} \in V_{\text{pw}}^1. \end{cases}$$

Second, the adjoints of the broken-FEEC differential operators associated *with* homogeneous boundary conditions, which should approximate the adjoint differential operators *without* boundary conditions: $\text{div}_{\text{pw}} := -(\mathbf{grad} P_0^0)^* : V_{\text{pw}}^1 \rightarrow V_{\text{pw}}^0$ and $\mathbf{curl}_{\text{pw}} := (\text{curl} P_0^1)^* : V_{\text{pw}}^2 \rightarrow V_{\text{pw}}^1$, defined by the relations

$$(2.17) \quad \begin{cases} \langle \phi, \text{div}_{\text{pw}} \mathbf{u} \rangle = -\langle \mathbf{grad} P_0^0 \phi, \mathbf{u} \rangle, & \forall \mathbf{u} \in V_{\text{pw}}^1, \phi \in V_{\text{pw}}^0, \\ \langle \mathbf{v}, \mathbf{curl}_{\text{pw}} w \rangle = \langle \text{curl} P_0^1 \mathbf{v}, w \rangle, & \forall w \in V_{\text{pw}}^2, \mathbf{v} \in V_{\text{pw}}^1. \end{cases}$$

We finally consider two kinds of patch-wise approximation operators, namely

$$(2.18) \quad \tilde{\Pi}_{\text{pw}}^\ell := (P^\ell)^* Q_{\text{pw}}^\ell : L^2(\Omega) \rightarrow V_{\text{pw}}^\ell \quad \text{and} \quad \tilde{\Pi}_{\text{pw},0}^\ell := (P_0^\ell)^* Q_{\text{pw}}^\ell : L^2(\Omega) \rightarrow V_{\text{pw}}^\ell$$

where Q_{pw}^ℓ is the L^2 -projection onto V_{pw}^ℓ . Then, one easily verifies (applying the definitions and integrating by parts as above) that the following relations hold:

$$\begin{cases} \text{div}_{\text{pw},0} \tilde{\Pi}_{\text{pw}}^1 \mathbf{u} = \tilde{\Pi}_{\text{pw}}^0 \text{div} \mathbf{u}, & \forall \mathbf{u} \in H_0(\text{div}; \Omega), \\ \mathbf{curl}_{\text{pw},0} \tilde{\Pi}_{\text{pw}}^2 \mathbf{v} = \tilde{\Pi}_{\text{pw}}^1 \mathbf{curl} \mathbf{v}, & \forall \mathbf{v} \in H_0(\mathbf{curl}; \Omega), \end{cases}$$

and

$$\begin{cases} \text{div}_{\text{pw}} \tilde{\Pi}_{\text{pw},0}^1 \mathbf{u} = \tilde{\Pi}_{\text{pw},0}^0 \text{div} \mathbf{u}, & \forall \mathbf{u} \in H(\text{div}; \Omega), \\ \mathbf{curl}_{\text{pw}} \tilde{\Pi}_{\text{pw},0}^2 \mathbf{v} = \tilde{\Pi}_{\text{pw},0}^1 \mathbf{curl} \mathbf{v}, & \forall \mathbf{v} \in H(\mathbf{curl}; \Omega). \end{cases}$$

Again, let us summarize the above observations in a formal statement.

Theorem 2.4. *Let $P^\ell : V_{\text{pw}}^\ell \rightarrow V_h^\ell$ and $P_0^\ell : V_{\text{pw}}^\ell \rightarrow V_{h,0}^\ell$ be discrete projection operators onto the conforming spaces without and with homogeneous boundary conditions, respectively. Then the discrete differential operators corresponding to (2.16), i.e.*

$$\text{div}_{\text{pw},0} := -(\mathbf{grad} P^0)^* : V_{\text{pw}}^1 \rightarrow V_{\text{pw}}^0, \quad \mathbf{curl}_{\text{pw},0} := (\text{curl} P^1)^* : V_{\text{pw}}^2 \rightarrow V_{\text{pw}}^1,$$

satisfy a commuting diagram

$$\begin{array}{ccccc} V_{\text{pw}}^0 & \xrightleftharpoons[\text{div}_{\text{pw},0}]{\mathbf{grad} P^0} & V_{\text{pw}}^1 & \xrightleftharpoons[\mathbf{curl}_{\text{pw},0}]{\text{curl} P^1} & V_{\text{pw}}^2 \\ \tilde{\Pi}_{\text{pw}}^0 \uparrow & & \tilde{\Pi}_{\text{pw}}^1 \uparrow & & \tilde{\Pi}_{\text{pw}}^2 \uparrow \\ L^2 & \xleftarrow{\text{div}} & H_0(\text{div}) & \xleftarrow{\mathbf{curl}} & H_0(\mathbf{curl}) \end{array}$$

where $\tilde{\Pi}_{\text{pw}}^\ell := (P^\ell)^* Q_{\text{pw}}^\ell$ is defined as in (2.18). Similarly, the discrete differential operators corresponding to (2.17), i.e.

$$\text{div}_{\text{pw}} := -(\mathbf{grad} P_0^0)^* : V_{\text{pw}}^1 \rightarrow V_{\text{pw}}^0, \quad \mathbf{curl}_{\text{pw}} := (\text{curl} P_0^1)^* : V_{\text{pw}}^2 \rightarrow V_{\text{pw}}^1,$$

satisfy a commuting diagram

$$\begin{array}{ccccc}
V_{\text{pw}}^0 & \xrightleftharpoons[\text{div}_{\text{pw}}]{\mathbf{grad} P_0^0} & V_{\text{pw}}^1 & \xrightleftharpoons[\mathbf{curl}_{\text{pw}}]{\mathbf{curl} P_0^1} & V_{\text{pw}}^2 \\
\tilde{\Pi}_{\text{pw},0}^0 \uparrow & & \tilde{\Pi}_{\text{pw},0}^1 \uparrow & & \tilde{\Pi}_{\text{pw},0}^2 \uparrow \\
L^2 & \xleftarrow[\text{div}]{} & H(\text{div}) & \xleftarrow[\mathbf{curl}]{} & H(\mathbf{curl})
\end{array}$$

where $\tilde{\Pi}_{\text{pw},0}^\ell := (P_0^\ell)^* Q_{\text{pw}}^\ell$ is defined as in (2.18). In particular, the boundary conditions associated with the weak differential operators are determined by the underlying conforming projection operator.

Let us observe that the operator $\tilde{\Pi}_{\text{pw}}^\ell = (P^\ell)^* Q_{\text{pw}}^\ell : L^2(\Omega) \rightarrow V_{\text{pw}}^\ell$ is a projection, but only onto a subspace of V_{pw}^ℓ : namely, onto $(P^\ell)^* V_{\text{pw}}^\ell$. For this projection to be a high order approximation operator, we see that $(P^\ell)^*$ must preserve the high order polynomials in V_{pw}^ℓ . In other terms, P^ℓ must preserve polynomial moments in logical coordinates.

Definition 2.5. An operator $P : V_{\text{pw}}^\ell \rightarrow V_{\text{pw}}^\ell$ is moment-preserving of order $r \geq 0$ if for any $u \in V_{\text{pw}}^\ell$ and any patch $k \in \mathcal{K}$, the pullbacks

$$\hat{u}_k = (\mathcal{F}_k^\ell)^{-1}((Pv)|_{\Omega_k}) \quad \text{and} \quad \hat{v}_k = (\mathcal{F}_k^\ell)^{-1}(v|_{\Omega_k})$$

satisfy the equalities

$$(2.19) \quad \langle \hat{u}_k, q \rangle = \langle \hat{v}_k, q \rangle$$

for all (scalar or vector valued) polynomials $q \in \mathbb{Q}_{r-1,r-1}[\hat{\mathbf{x}}]$ defined on the logical domain $\hat{\Omega}$.

Remark 2.6. In the case $r = 0$, we have $\mathbb{Q}_{r-1,r-1}[\hat{\mathbf{x}}]_{-1,-1} = \{0\}$ and the prior definition is empty. For this reason we may say that the operator is not moment-preserving.

Remark 2.7. The L^2 -projection operator $Q_{\text{pw}}^\ell : L^2(\Omega) \rightarrow V_{\text{pw}}^\ell$ defined by

$$\langle Q_{\text{pw}}^\ell v, u \rangle = \langle v, u \rangle, \quad \forall v \in L^2(\Omega), \quad \forall u \in V_{\text{pw}}^\ell,$$

is moment-preserving of order $p+1$ for $\ell = 0$, and of order p for $\ell \geq 1$, reminding that p is the polynomial degree of the discrete space V^0 . Given the form of $\tilde{\Pi}_{\text{pw}}^\ell$ above, it is then natural to design conforming projection operators P^ℓ that preserve moments of order $r = r(P^\ell)$ with $r(P^0) \leq p+1$ and $r(P^1) \leq p$.

2.6. Broken-FEEC discretizations of model PDEs. For the numerical verification of our conforming projection operators, we revise the test problems and numerical schemes of the broken-FEEC framework from [26, Section 3].

2.6.1. Broken degrees of freedom. Following [26, Section 2.4], we assume that each local space V_k^ℓ is equipped with linear forms

$$(2.20) \quad \sigma_{\mathbf{i}}^{\ell,k} : V_k^\ell \rightarrow \mathbb{R}, \quad \mathbf{i} \in \mathcal{I}^{\ell,k},$$

which are characterized by duality to the basis functions:

$$\sigma_{\mathbf{i}}^{\ell,k}(\Lambda_{\mathbf{j}}^{\ell,k}) = \delta_{\mathbf{i},\mathbf{j}}, \quad \mathbf{i}, \mathbf{j} \in \mathcal{I}^{\ell,k}.$$

In the numerical examples of Section 5, we will use B-spline basis functions so that σ in (2.20) are their corresponding coefficients.

This allows for the description of the differential operators in matrix form onto the coefficients, also called degrees of freedom (DOF), of the patch-local basis functions. For ease of notation, we will reduce/flatten the tuple of patch index $k \in \mathcal{K}$ and multi-index $\mathbf{i} \in \mathcal{I}^{\ell,k}$ to a single index

$$m : (k, \mathbf{i}) \mapsto m \in \{1, \dots, N^\ell := \dim(V_{\text{pw}}^\ell)\},$$

such that $\Lambda_m^\ell = \Lambda_{\mathbf{i}}^{\ell,k}$.

The differential operators **grad** and **curl** in matrix form are then given by

$$\begin{aligned} \mathbf{G}_{i,j} &= \sigma_i^1(\mathbf{grad}_{\text{pw}} \Lambda_j^0), \quad i = 1, \dots, N^1, j = 1, \dots, N^0, \\ \mathbf{C}_{i,j} &= \sigma_i^2(\mathbf{curl}_{\text{pw}} \Lambda_j^1), \quad i = 1, \dots, N^2, j = 1, \dots, N^1. \end{aligned}$$

These matrices are of sizes $N^1 \times N^0$ and $N^2 \times N^1$ respectively with a patch-diagonal structure, that means the matrices are block-diagonal with blocks corresponding to the patch-local differential operator.

The conforming projection (2.9) as an endomorphism on V_{pw}^0 in matrix form reads

$$\mathbf{P}_{i,j}^\ell = \sigma_i^\ell(P^\ell \Lambda_j^\ell), \quad i, j = 1, \dots, N^\ell.$$

Since the conforming projection P^ℓ maps into the conforming space V_h^ℓ , the matrix \mathbf{P}^ℓ is not block diagonal, but has to average/couple degrees of freedom on shared interfaces.

Introducing the coefficient spaces $\mathcal{C}^\ell = \mathbb{R}^{N^\ell}$, we can write the commuting diagram:

$$\begin{array}{ccccc} V_{\text{pw}}^0 & \xrightarrow{\mathbf{grad} P^0} & V_{\text{pw}}^1 & \xrightarrow{\mathbf{curl} P^1} & V_{\text{pw}}^2 \\ \downarrow \sigma^0 & & \downarrow \sigma^1 & & \downarrow \sigma^2 \\ \mathcal{C}^0 & \xrightarrow{\mathbf{GP}^0} & \mathcal{C}^1 & \xrightarrow{\mathbf{CP}^1} & \mathcal{C}^2 \end{array}$$

For other purposes, such as the coderivative matrices, we also need the mass-matrices \mathbf{M}^ℓ , which are defined as

$$\mathbf{M}_{i,j}^\ell = \langle \Lambda_i^\ell, \Lambda_j^\ell \rangle_{L^2(\Omega)}, \quad i, j = 1, \dots, N^\ell,$$

and are block-diagonal as well. Another matrix that we will use is the identity matrix \mathbf{I} , which is the identity operator on the coefficient space \mathcal{C}^ℓ depending on the context.

2.6.2. Weak differential operators. Using the definitions in Section 2.5, we can write the weak differential operators in the broken-FEEC framework, they then read

$$\tilde{\mathbf{D}} = -(\mathbf{M}^0)^{-1} (\mathbf{GP}^0)^T \mathbf{M}^1,$$

and

$$\tilde{\mathbf{C}} = -(\mathbf{M}^1)^{-1} (\mathbf{CP}^1)^T \mathbf{M}^2.$$

In Section 5.1, we verify the approximation properties of these weak differential operators, as we apply them to smooth test functions and compare them to the exact differentials.

2.6.3. Poisson problem. Following [26, Section 3.1], we consider the Poisson problem with homogeneous boundary conditions, i.e. for given $f \in L^2(\Omega)$, find $\phi \in V^0 = H_0^1(\Omega)$ such that

$$-\Delta\phi = f.$$

Within the broken-FEEC Framework, this equation is discretized as

$$\left((\mathbf{GP}^0)^T \mathbf{M}^1 \mathbf{GP}^0 + \alpha \underbrace{(\mathbf{I} - \mathbf{P}^0)^T \mathbf{M}^0 (\mathbf{I} - \mathbf{P}^0)}_{\text{jump stabilization}} \right) \boldsymbol{\phi} = (\mathbf{P}^0)^T \mathbf{M}^0 \mathbf{f},$$

for some $\alpha > 0$, the coefficients $\mathbf{f} \in \mathcal{C}^0$ of a projection of the source f and the coefficients $\boldsymbol{\phi} \in \mathcal{C}^0$ of the solution ϕ . Notice that the right-hand-side is obtained by a filtered L^2 -projection similar to in Section 2.5.

2.6.4. Time-harmonic Maxwell problem. In order to study the time-harmonic Maxwells problem with inhomogeneous boundary conditions, we again follow [26, Section 3.3]: For $\omega \in \mathbb{R}$ and $\mathbf{J} \in L^2(\Omega)$, we solve

$$-\omega^2 \mathbf{E} + \mathbf{curl} \mathbf{curl} \mathbf{E} = \mathbf{J},$$

for $\mathbf{E} \in V^1 = H(\mathbf{curl}, \Omega)$. In our framework, that reads

$$\left(-\omega^2 (\mathbf{P}^1)^T \mathbf{M}^1 \mathbf{P}^1 + (\mathbf{CP}^1)^T \mathbf{M}^2 \mathbf{CP}^1 + \alpha \underbrace{(\mathbf{I} - \mathbf{P}^1)^T \mathbf{M}^1 (\mathbf{I} - \mathbf{P}^1)}_{\text{jump stabilization}} \right) \mathbf{e} = (\mathbf{P}^1)^T \mathbf{M}^1 \mathbf{j},$$

for some $\alpha > 0$, with the discrete source coefficients $\mathbf{j} \in \mathcal{C}^1$ and the solution coefficients $\mathbf{e} \in \mathcal{C}^1$.

2.6.5. Curl-curl eigenvalue problem. Following [26, Section 3.4 and Section 5.5], we look at the spectral correctness of the \mathbf{curl} -curl eigenvalue problem: Find $\lambda > 0$ such that

$$\mathbf{curl} \mathbf{curl} \mathbf{E} = \lambda \mathbf{E},$$

where $\mathbf{E} \in V^1 = H_0(\mathbf{curl}, \Omega)$.

Within the broken-FEEC framework, this equation is discretized as

$$(\mathbf{CP}^1)^T \mathbf{M}^2 \mathbf{CP}^1 \mathbf{e} = \lambda \left(\alpha \underbrace{(\mathbf{I} - \mathbf{P}^1)^T \mathbf{M}^1 (\mathbf{I} - \mathbf{P}^1)}_{\text{jump stabilization}} + (\mathbf{P}^1)^T \mathbf{M}^1 \mathbf{P}^1 \right) \mathbf{e},$$

for $\alpha > 0$ and with the coefficients $\mathbf{e} \in \mathcal{C}^1$.

2.6.6. *Time-domain Maxwell.* We consider the time-domain Maxwell problem on a square domain as described in [26, Section 3.6 and Section 5.7]: For $\mathbf{J} \in L^2(\Omega)$, solve

$$\begin{aligned}\partial_t \mathbf{E} - \mathbf{curl} B &= -\mathbf{J}, \\ \partial_t B + \mathbf{curl} \mathbf{E} &= 0,\end{aligned}$$

where $\mathbf{E} \in H_0(\mathbf{curl}, \Omega)$ and $B \in L^2(\Omega)$. A semi-discrete scheme in the broken-FEEC framework then reads

$$(2.21) \quad \begin{aligned}\mathbf{M}^1 \partial_t \mathbf{e} &= (\mathbf{CP}^1)^T \mathbf{M}^2 \mathbf{b} - (\mathbf{P}^1)^T \mathbf{M}^1 \mathbf{j}, \\ \partial_t \mathbf{b} &= -\mathbf{CP}^1 \mathbf{e},\end{aligned}$$

with coefficients $\mathbf{b} \in \mathcal{C}^0$, $\mathbf{e} \in \mathcal{C}^1$ and $\mathbf{j} \in \mathcal{C}^1$. This will be put in a fully discrete scheme by using a leapfrog time-stepping scheme later on.

2.6.7. *Time-domain Helmholtz.* Analogous to the time-domain Maxwell problem, we consider the Helmholtz equation and solve

$$\begin{aligned}\partial_t \phi - \operatorname{div} \mathbf{U} &= 0, \\ \partial_t \mathbf{U} + \mathbf{grad} \phi &= 0,\end{aligned}$$

for $\phi \in H_0^1(\Omega)$ and $\mathbf{U} \in H(\operatorname{div}, \Omega)$. Similar to before, the semi-discrete scheme reads

$$\begin{aligned}\mathbf{M}^0 \partial_t \phi &= (\mathbf{GP}^0)^T \mathbf{M}^1 \mathbf{u}, \\ \partial_t \mathbf{u} &= -\mathbf{GP}^0 \phi,\end{aligned}$$

where $\phi \in \mathcal{C}^0$ and $\mathbf{u} \in \mathcal{C}^1$ and will be fully discretized later on.

3. CONFORMING PROJECTION OPERATORS ON V_{pw}^0

On the first space of (2.1), where the H^1 -conformity amounts to continuity of functions across all patches as described in Section 2.3, the discrete conforming space is defined as $V_h^0 = V_{\text{pw}}^0 \cap H^1(\Omega)$. We construct a conforming projection

$$P^0 : V_{\text{pw}}^0 \rightarrow V_{\text{pw}}^0$$

onto the space V_h^0 by averaging degrees of freedom of interface basis functions. In our approach, we first ensure continuity at domain vertex basis functions by applying a vertex-based conforming projection $P_{\mathcal{V}}$. Subsequently, we apply an edge-based conforming projection $P_{\mathcal{E}}$ for continuity along edge-interior basis functions. The first operation is straightforward, but the second one involves extension and restriction operators, mapping to the shared interface-spaces, introduced in Section 3.2, since the patch resolutions may be different across the edges. In addition to the averaging procedure that enforces the continuity at the patch interfaces, we complete our projection operators with local correction terms in order to preserve polynomial moments. A benefit of this approach is to allow for a local and fully decoupled treatment of vertices and edges. For the clarity of the presentation, we first list some properties of the vertex- and edge-based projection operators that will be discussed in the following Section 3.1 and Section 3.2.

Proposition 3.1. Given $\phi \in V_{\text{pw}}^0$, $v \in \mathcal{V}$, and let the order of moment preservation be $r = r(P^0)$ with $0 \leq r \leq p + 1$, then the local vertex-based operator $P_v : V_{\text{pw}}^0 \rightarrow V_{\text{pw}}^0$ defined in (3.5) below satisfies the following properties

- (1) $P_v \phi$ is continuous at v .
- (2) $P_v \phi = \phi$ if and only if ϕ is continuous at v .
- (3) P_v preserves polynomial moments of order r in the sense of Definition 2.5.
- (4) $P_v P_{v'} \phi = P_{v'} P_v \phi$ for any $v' \in \mathcal{V}$.

Proposition 3.2. Given $\phi \in V_{\text{pw}}^0$ that is continuous on vertices, $e \in \mathcal{E}$, and let the order of moment preservation be $r = r(P^0)$ with $0 \leq r \leq p + 1$, then the local edge-based operator $P_e : V_{\text{pw}}^0 \rightarrow V_{\text{pw}}^0$ defined in (3.8) below satisfies the following properties

- (1) $P_e \phi$ is continuous on e .
- (2) $P_e \phi = \phi$ if and only if ϕ is continuous on e .
- (3) P_e preserves polynomial moments of order r in the sense of Definition 2.5.
- (4) $P_e P_{e'} \phi = P_{e'} P_e \phi$ for any $e' \in \mathcal{E}$.

Combining both allows us to define the full V^0 conforming projection:

Theorem 3.3. *Defining the vertex- and edge-based operators*

$$(3.1) \quad P_{\mathcal{V}} = \prod_{v \in \mathcal{V}} P_v, \quad P_{\mathcal{E}} = \prod_{e \in \mathcal{E}} P_e,$$

consisting of the local operators (3.5) and (3.8), then

$$P^0 = P_{\mathcal{E}} P_{\mathcal{V}} : V_{\text{pw}}^0 \rightarrow V_{\text{pw}}^0$$

is a projection onto the conforming space V_h^0 which is moment-preserving of order $0 \leq r \leq p + 1$.

Proof. Note that the products in (3.1) are well-defined, as their order does not matter thanks to (4) in Proposition 3.1 and Proposition 3.2. For the range property of P^0 , let $\phi \in V_{\text{pw}}^0$ and write $\tilde{\phi} = P_V \phi$, which is continuous at any vertex by (1) in Proposition 3.1. This continuity is conserved by $P_{\mathcal{E}}$, and $P_{\mathcal{E}} \tilde{\phi}$ is additionally continuous on any edge by (1) in Proposition 3.2. Thus, P^0 maps into the continuous space V_h^0 . The projection property of P^0 directly follows from (2) in Proposition 3.1 and Proposition 3.2. Using (3) in Proposition 3.1 and Proposition 3.2, since every operator in the composition preserves polynomial moments, we can directly infer the moment preservation property of the product. \square

3.1. Vertex-based projections. In this section, we detail the construction of the vertex conforming projection of Proposition 3.1 resulting in Definition 3.5. Let the order of moment preservation be given by $0 \leq r \leq p + 1$ and fix a vertex $v \in \mathcal{V}$. For ease of notation, assume that the ordering of basis functions of V_k^0 , c.f. (2.13), in every adjacent patch $k \in \mathcal{K}(v)$ starts with the one basis function on the vertex v , i.e. $\Lambda_{\mathbf{0}}^k$ is associated to v for all $k \in \mathcal{K}(v)$.

Local vertex conforming projection. We define the local vertex conforming projection P_v that establishes continuity at the vertex v . In absence of moment-preservation ($r = 0$) this is done by mapping the patch-wise basis functions associated to the vertex v (one per patch) to the same degree of freedom, averaged in order to become a projection:

$$(3.2) \quad P_v = \Lambda_j^k \mapsto \begin{cases} \bar{\Lambda}^v & \text{if } j = \mathbf{0} \text{ and } k \in \mathcal{K}(v), \\ \Lambda_j^k & \text{else,} \end{cases}$$

where $k \in \mathcal{K}$ and we define the vertex-conforming function $\bar{\Lambda}^v$ as the average of the patch-wise basis functions at the vertex:

$$(3.3) \quad \bar{\Lambda}^v = \frac{1}{\#\mathcal{K}(v)} \sum_{k' \in \mathcal{K}(v)} \Lambda_{\mathbf{0}}^{k'},$$

with $\#\mathcal{K}(v)$ being the number of patches sharing the vertex v .

Preservation of polynomial moments. In the case where $r \geq 1$, we need to add correction terms to the definition of P_v in (3.2). Following Definition 2.5, we choose correction terms that involve additional interior degrees of freedom, and we use those that are close to the vertex and that preserve the continuity. So for any patch $k \in \mathcal{K}(v)$, we consider the ansatz

$$(3.4) \quad P_v \Lambda_{\mathbf{0}}^k = \bar{\Lambda}^v + \sum_{m_1, m_2=1}^r \mathbf{a}_m \Lambda_m^k + \sum_{\substack{k' \in \mathcal{K}(v) \\ k' \neq k}} \sum_{m_1, m_2=1}^r \tilde{\mathbf{a}}_m \Lambda_m^{k'},$$

with coefficients $\mathbf{a}_m = a_{1, m_1} a_{2, m_2}$ – similarly $\tilde{\mathbf{a}}_m$ – to be determined. As we will see later, specifically in Remark 3.4, these correction terms can be determined independently of the patch, which is an important property of our construction and allows us to omit a patch-dependent notation here. In the case $r = 0$, this ansatz is consistent with the prior definition.

The pullbacks on the patch Ω_k read

$$\begin{aligned} (\mathcal{F}_k^0)^{-1}(\Lambda_{\mathbf{i}}^k|_{\Omega_k}) &= \hat{\Lambda}_{\mathbf{i}}^k, \quad (\mathcal{F}_k^0)^{-1}(\Lambda_{\mathbf{i}}^{k'}|_{\Omega_k}) = 0, \\ (\mathcal{F}_k^0)^{-1}(P_v \Lambda_{\mathbf{0}}^k|_{\Omega_k}) &= \frac{1}{\#\mathcal{K}(v)} \hat{\Lambda}_{\mathbf{0}}^k + \sum_{m_1, m_2=1}^r \mathbf{a}_m \hat{\Lambda}_m^k, \end{aligned}$$

which allows us to write (2.19), for any $q(\hat{\mathbf{x}}) = q_1(\hat{\mathbf{x}}_1)q_2(\hat{\mathbf{x}}_2) \in \mathbb{Q}_{r-1, r-1}[\hat{\mathbf{x}}]$ as

$$\begin{aligned} & \int_{\hat{\Omega}} \left(\frac{1}{\#\mathcal{K}(v)} \hat{\Lambda}_{\mathbf{0}}^k + \sum_{m_1, m_2=1}^r \mathbf{a}_m \hat{\Lambda}_m^k \right) q = \int_{\hat{\Omega}} \hat{\Lambda}_{\mathbf{0}}^k q \\ \Leftrightarrow & \sum_{m_1, m_2=1}^r \mathbf{a}_m \int_{\hat{\Omega}} \hat{\Lambda}_m^k q = \left(1 - \frac{1}{\#\mathcal{K}(v)} \right) \int_{\hat{\Omega}} \hat{\Lambda}_{\mathbf{0}}^k q \\ \Leftarrow & \sum_{m=1}^r a_{t,m} \int_0^1 \lambda_m^k q_t = \sqrt{1 - \frac{1}{\#\mathcal{K}(v)}} \int_0^1 \lambda_0^k q_t, \quad \text{for } t = 1, 2, \end{aligned}$$

by the tensor-product structure of the basis functions (2.13). On the other hand, on any patch $\Omega_{k'}$ with $k' \in \mathcal{K}(v) \setminus \{k\}$, we have the pullbacks

$$\begin{aligned} (\mathcal{F}_{k'}^0)^{-1}(\Lambda_{\mathbf{i}}^{k'}|_{\Omega_{k'}}) &= \hat{\Lambda}_{\mathbf{i}}^{k'}, \quad (\mathcal{F}_{k'}^0)^{-1}(\Lambda_{\mathbf{i}}^k|_{\Omega_{k'}}) = 0, \\ (\mathcal{F}_{k'}^0)^{-1}(P_v \Lambda_{\mathbf{0}}^{k'}|_{\Omega_{k'}}) &= \frac{1}{\#\mathcal{K}(v)} \hat{\Lambda}_{\mathbf{0}}^{k'} + \sum_{m_1, m_2=1}^r \tilde{\mathbf{a}}_m \hat{\Lambda}_m^{k'}, \end{aligned}$$

and thus for any $q(\hat{\mathbf{x}}) = q_1(\hat{\mathbf{x}}_1)q_2(\hat{\mathbf{x}}_2) \in \mathbb{Q}_{r-1, r-1}[\hat{\mathbf{x}}]$:

$$\begin{aligned} & \int_{\hat{\Omega}} \left(\frac{1}{\#\mathcal{K}(v)} \hat{\Lambda}_{\mathbf{0}}^{k'} + \sum_{m_1, m_2=1}^r \tilde{\mathbf{a}}_m \hat{\Lambda}_m^{k'} \right) q = 0 \\ \Leftrightarrow & \sum_{m_1, m_2=1}^r \tilde{\mathbf{a}}_m \int_{\hat{\Omega}} \hat{\Lambda}_m^{k'} q = -\frac{1}{\#\mathcal{K}(v)} \int_{\hat{\Omega}} \hat{\Lambda}_{\mathbf{0}}^{k'} q \\ \Leftarrow & \sum_{m=1}^r \tilde{a}_{t,m} \int_0^1 \lambda_m^{k'} q_t = (-1)^t \sqrt{\frac{1}{\#\mathcal{K}(v)}} \int_0^1 \lambda_0^{k'} q_t, \quad \text{for } t = 1, 2. \end{aligned}$$

Now, we can solve the linear system for the correction coefficients \mathbf{a} and $\tilde{\mathbf{a}}$. Let $(q_j)_{1 \leq j \leq r}$ be the basis of the univariate polynomial space $\mathbb{Q}_{r-1}[\hat{x}]$ and define the basis-polynomial duality-matrices and vertex-basis-polynomial vectors as

$$(3.5) \quad \mathbf{M}^k = \left(\int_0^1 \lambda_m^k q_j \right)_{1 \leq m \leq r, 1 \leq j \leq r}, \quad \mathbf{b}^k = \left(\int_0^1 \lambda_0^k q_j \right)_{1 \leq j \leq r}.$$

We can thus write the linear systems as

$$\mathbf{M}^k a_t = \sqrt{1 - \frac{1}{\#\mathcal{K}(v)}} \mathbf{b}^k, \quad \mathbf{M}^{k'} \tilde{a}_t = (-1)^t \sqrt{\frac{1}{\#\mathcal{K}(v)}} \mathbf{b}^{k'},$$

and solve them for

$$\mathbf{a} = \left(1 - \frac{1}{\#\mathcal{K}(v)} \right) (\mathbf{M}^k)^{-1} \mathbf{b}^k \otimes (\mathbf{M}^k)^{-1} \mathbf{b}^k, \quad \tilde{\mathbf{a}} = -\frac{1}{\#\mathcal{K}(v)} (\mathbf{M}^{k'})^{-1} \mathbf{b}^{k'} \otimes (\mathbf{M}^{k'})^{-1} \mathbf{b}^{k'}.$$

Remark 3.4. As announced above, we verify that the coefficients \mathbf{a} , $\tilde{\mathbf{a}}$ are independent of the mappings F_k , $F_{k'}$ and only depend on the logical basis of \mathbb{V}^0 . Since we assumed nestedness of the patches, e.g. by some refinement factor say 2^θ ($\theta \in \mathbb{Z}$) between the resolutions of patch k and k' , we have a scaling relation between one-dimensional basis functions on the logical tensor-product domain:

$$\lambda_i^k(x) = \lambda_{i'}^{k'}(2^\theta x).$$

Performing a change of basis in (3.5) by $q_j(x) = \tilde{q}_j(2^\theta x)$, i.e.

$$(3.6) \quad \int_0^1 \lambda_i^k q_j = \int_0^1 \frac{\lambda_{i'}^{k'} \tilde{q}_j}{2^\theta},$$

and defining the one-dimensional correction coefficient

$$(3.7) \quad \gamma^{1d} = (\mathbf{M}^k)^{-1} \mathbf{b}^k \in \mathbb{R}^r,$$

we realize that this definition is independent of the patch k and direction t because the scaling factor from (3.6) cancels.

Thus, we can define the correction coefficient

$$(3.8) \quad \gamma = \gamma^{1d} \otimes \gamma^{1d}$$

independent of the patch $k \in \mathcal{K}(\mathbf{v})$ and its mapping F_k , which is an important property of our construction, and more elegantly write

$$\mathbf{a} = \left(1 - \frac{1}{\#\mathcal{K}(\mathbf{v})}\right) \gamma, \quad \tilde{\mathbf{a}} = -\frac{1}{\#\mathcal{K}(\mathbf{v})} \gamma.$$

The full operator for a given vertex \mathbf{v} resulting from this construction then reads:

Definition 3.5. The local vertex conforming projection $P_{\mathbf{v}} : V_{\text{pw}}^0 \rightarrow V_{\text{pw}}^0$ is defined as

$$P_{\mathbf{v}} : \Lambda_{\mathbf{j}}^k \mapsto \begin{cases} \bar{\Lambda}^{\mathbf{v}} + \sum_{m_1, m_2=1}^r \gamma_{\mathbf{m}} \left(\Lambda_{\mathbf{m}}^k - \frac{1}{\#\mathcal{K}(\mathbf{v})} \sum_{k' \in \mathcal{K}(\mathbf{v})} \Lambda_{\mathbf{m}}^{k'} \right) & \text{if } \mathbf{j} = \mathbf{0} \text{ and } k \in \mathcal{K}(\mathbf{v}), \\ \Lambda_{\mathbf{j}}^k & \text{else,} \end{cases}$$

for all $\mathbf{j} \in \mathbf{I}^k$, where $\Lambda_{\mathbf{j}}^k$ are the patch-wise basis functions defined in equation (2.13), the order of moment preservation is $0 \leq r \leq p+1$, γ the correction coefficients in (3.8) and $\bar{\Lambda}^{\mathbf{v}}$ the vertex-conforming basis function in (3.3).

Remark 3.6. Since

$$r \leq p+1 < p + N_k - 1 = n_k$$

which holds by Assumption 2.1, the correction terms do not involve other vertex basis functions (which have one index n_k). Again, recall that for $r = 0$, the sum is vanishing, and we are consistent with the prior definition.

Now, we are in the position to prove Proposition 3.1.

Proof of Proposition 3.1.

- (1) In order to show that $P_v \phi$ is continuous at v , let $\phi = \sum_k \sum_i \phi_i^k \Lambda_i^k \in V_{pw}^0$ and $v \in \mathcal{V}$, we write its projection restricted to a patch $\Omega_{k'}, k' \in \mathcal{K}(v)$ as

$$\begin{aligned} (P_v \phi)|_{\Omega_{k'}}(v) &= \sum_{k \in \mathcal{K}(v)} \sum_i \phi_i^k (P_v \Lambda_i^k)|_{\Omega_{k'}}(v) \\ &= \sum_{k \in \mathcal{K}(v)} \phi_0^k \bar{\Lambda}^v|_{\Omega_{k'}}(v) \\ &= \sum_{k \in \mathcal{K}(v)} \frac{\phi_0^k}{\#\mathcal{K}(v)} \underbrace{\Lambda_0^{k'}(v)}_{=1} \end{aligned}$$

where we only mapped the vertex basis functions as the others vanish, the same holds true for the moment correction terms. Thus, since the restriction to any patch $k' \in \mathcal{K}(v)$ yields the same value, the projection $P_v \phi$ is continuous at v .

- (2) Next, we want to show: $P_v \phi = \phi$ if and only if ϕ is continuous at v . The first direction, namely " \Rightarrow ", directly follows from (1). For the other direction, let $\phi = \sum_k \sum_i \phi_i^k \Lambda_i^k \in V_{pw}^0$ be continuous at the vertex v , we denote by

$$\phi_0 = \phi_0^k = \frac{1}{\#\mathcal{K}(v)} \sum_{l \in \mathcal{K}(v)} \phi_0^l, \quad \forall k \in \mathcal{K}(v),$$

the common coefficient of the vertex basis function on each patch and thus the projection reads

$$\begin{aligned} P_v \phi &= \sum_{k \in \mathcal{K}(v)} \sum_{i \neq 0} \phi_i^k \Lambda_i^k + \sum_{k \in \mathcal{K}(v)} \phi_0^k P_v \Lambda_0^k \\ &= \sum_{k \in \mathcal{K}(v)} \sum_{i \neq 0} \phi_i^k \Lambda_i^k + \phi_0 \sum_{k \in \mathcal{K}(v)} \left(\bar{\Lambda}^v + \sum_{m_1, m_2=1}^r \gamma_m \left(\Lambda_m^k - \frac{1}{\#\mathcal{K}(v)} \sum_{k' \in \mathcal{K}(v)} \Lambda_m^{k'} \right) \right) \\ &= \sum_{k \in \mathcal{K}(v)} \sum_{i \neq 0} \phi_i^k \Lambda_i^k + \phi_0 \left(\#\mathcal{K}(v) \bar{\Lambda}^v + \sum_{m_1, m_2=1}^r \gamma_m \underbrace{\left(\sum_{k \in \mathcal{K}(v)} \Lambda_m^k - \sum_{k' \in \mathcal{K}(v)} \Lambda_m^{k'} \right)}_{=0} \right) \\ &= \sum_{k \in \mathcal{K}(v)} \sum_{i \neq 0} \phi_i^k \Lambda_i^k + \phi_0 \sum_{k \in \mathcal{K}(v)} \Lambda_0^k \\ &= \sum_{k \in \mathcal{K}(v)} \sum_{i \neq 0} \phi_i^k \Lambda_i^k + \phi_0 \Lambda_0^k = \phi \end{aligned}$$

- (3) The preservation of polynomial moments holds by construction in Section 3.1.
- (4) The vertex-based operators for different vertices are commuting since by Remark 3.6, the projection P_v does not change coefficients of other vertex basis functions.

□

3.2. Edge-based projections. For this section, we again let the moment preservation order be given by $0 \leq r \leq p + 1$, fix an interface $e \in \mathcal{E}$ and denote by $k^- \in \mathcal{K}(e)$ (or in exponents just $-$) the coarse and $k^+ \in \mathcal{K}(e)$ (or in exponents just $+$) the fine patch adjacent to the edge e . Since the ordering of the patch-wise basis functions depends on the orientation of the edge, we have to distinguish between vertical and horizontal interfaces, but without loss of generality we can assume for the following definitions that the first index is the edge parallel coordinate and the second index the edge perpendicular coordinate, i.e.

$$\mathbf{j} = (j_1, j_2), \quad j_1 = j_{\parallel(\hat{e})}, \quad j_2 = j_{\perp(\hat{e})}.$$

Furthermore, we assume that for both patches the basis functions in the edge-perpendicular direction are ordered starting with the edge-basis functions associated with the edge e . At the same time, we assume that the basis functions in the edge-parallel direction are ordered in the same direction on both adjacent patches.

As another ease of notation, we consider a (edge) local parametrization of the patches k^- and k^+ consisting of a single mapping $F = F(e) : \hat{\Omega}(e) \rightarrow \Omega(e)$, such that the edge-local logical domain $\hat{\Omega}(e) = [0, 1] \times [1, -1]$, is the juxtaposition of the tensor-product patches $\hat{\Omega}_{\pm}$, and the edge-local physical domain $\Omega(e)$, to be the juxtaposition of the physical patches Ω_{\pm} . An illustration is provided in Figure 1.

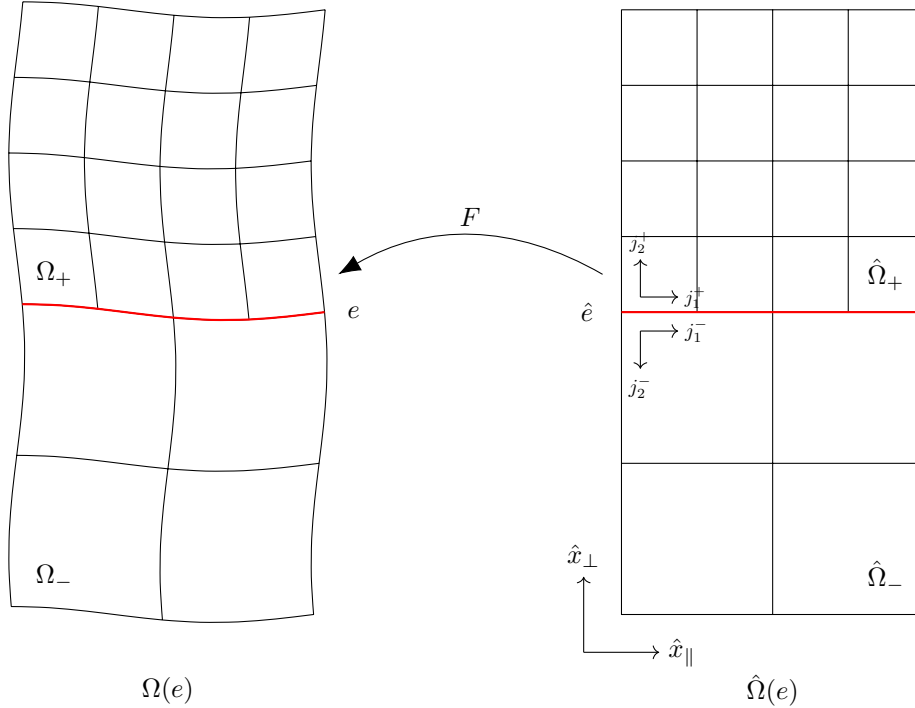


FIGURE 1. The edge-local logical domain $\hat{\Omega}(e)$ (right) and the edge-local physical domain $\Omega(e)$ (left) for a horizontal edge e , different resolutions and the mapping $F(e)$. Additionally, we show the orientation of the logical variables and indicate the direction of increasing basis index ordering.

This allows us to extend the patch-wise logical basis functions in edge-perpendicular direction to the whole edge-local logical domain $\hat{\Omega}(e)$:

(3.9)

$$\lambda_{\perp,i}^-(\hat{x}_{\perp}) = \begin{cases} \lambda_i^-(-\hat{x}_{\perp}) & \text{if } -1 \leq \hat{x}_{\perp} \leq 0 \\ 0 & \text{if } 0 < \hat{x}_{\perp} \leq 1 \end{cases}, \quad \lambda_{\perp,i}^+(\hat{x}_{\perp}) = \begin{cases} 0 & \text{if } -1 \leq \hat{x}_{\perp} \leq 0 \\ \lambda_i^+(\hat{x}_{\perp}) & \text{if } 0 < \hat{x}_{\perp} \leq 1 \end{cases}$$

for all $0 < i < n_{\pm}$. On the other hand, the nested univariate function spaces along the edge \hat{e} , i.e. $\hat{V}_{\pm,\parallel}^0 = \mathbb{V}_{\pm}^0$, are naturally defined on the edge-local logical domain $\hat{\Omega}(e)$, but have to be corrected for continuity by the conforming projection as they in general have different resolutions.

Extension-Restriction operators. In order to combine spline spaces of different refinement levels on shared interfaces, we introduce projections between the univariate logical edge-parallel function spaces $\hat{V}_{\pm,\parallel}^0 = \mathbb{V}_{\pm}^0$. We refer to them as extension operators \mathcal{E} (inclusion/change of basis) when mapping a coarse to a fine spline, and restriction operators \mathcal{R} (L^2 -projection) for the opposite direction.

We define the extension operator \mathcal{E} , projecting coarse one-dimensional spline functions to fine ones, as a map

$$(3.10) \quad \mathcal{E} : \mathbb{V}_{-}^0 \subset \mathbb{V}_{+}^0 \longrightarrow \mathbb{V}_{+}^0,$$

that acts as the change of basis describing the (coarse) basis functions of \mathbb{V}_{-}^0 in the (fine) basis of \mathbb{V}_{+}^0 , which is possible due to Assumption 2.2. Its matrix form \mathbf{E} , the change of basis matrix, is defined in Section B.2.

Constructing the restriction operator \mathcal{R} is more involved as we want to define a projection from the fine to the coarse spline space:

$$(3.11) \quad \mathcal{R} : \mathbb{V}_{+}^0 \longrightarrow \mathbb{V}_{-}^0 \subset \mathbb{V}_{+}^0,$$

naturally this will be a left inverse of the extension operator, i.e. $\mathcal{R}\mathcal{E} = \text{id}$. Since the edge local conforming projection should not change the vertex degrees of freedom, as we mentioned in the beginning, we have additional constraints:

$$(3.12) \quad \mathcal{R}\lambda_0^+(0) = \mathcal{R}\lambda_0^-(0) = \lambda_0^-(0), \quad \mathcal{R}\lambda_{n_+}^+(1) = \mathcal{R}\lambda_{n_-}^-(1) = \lambda_{n_-}^-(1).$$

First, we introduce the interior spaces $\mathbb{V}_{\pm,0}^0 = \text{Span}(\{\lambda_i^{\pm} \mid 0 < i < n_{\pm}\})$ and write the restriction operator as

$$(3.13) \quad \mathcal{R}\hat{\phi} = (\text{id} - \mathcal{T})\hat{\phi} + \mathcal{R}_0\mathcal{T}\hat{\phi},$$

depending on the interior restriction operator \mathcal{R}_0 constructed below, and where the truncation $\mathcal{T} : \mathbb{V}_{+}^0 \longrightarrow \mathbb{V}_{+,0}^0$ is defined as

$$(3.14) \quad \mathcal{T}\hat{\phi} = \hat{\phi} - \hat{\phi}_0\lambda_0^- - \hat{\phi}_{n_+}\lambda_{n_-}^-,$$

note that $(\mathcal{T}\hat{\phi})(0) = (\mathcal{T}\hat{\phi})(1) = 0$ as the basis functions are interpolatory at the boundaries. The interior restriction operator $\mathcal{R}_0 : \mathbb{V}_{+,0}^0 \longrightarrow \mathbb{V}_{-,0}^0$ is defined on the interior fine space and thus does not involve vertex degrees of freedom. This interior restriction operator \mathcal{R}_0 is defined using the full L^2 -projection $\tilde{\mathcal{R}}$ from the interior fine space $\mathbb{V}_{+,0}^0$ onto the coarse space \mathbb{V}_{-}^0 :

$$(3.15) \quad \int \lambda_j^- \tilde{\mathcal{R}}\lambda_i^+ = \int \lambda_j^- \lambda_i^+, \quad \forall j = 0, \dots, n_-, i = 1, \dots, n_+ - 1,$$

which is moment preserving since \mathbb{V}_\pm^0 contains all polynomials of degree $p \geq r-1$ as mentioned in Remark 2.7. But in order to remove the vertex degrees of freedom from the range of the projection in a moment preserving way, we introduce another truncation $\tilde{\mathcal{T}} : \mathbb{V}_-^0 \rightarrow \mathbb{V}_{-,0}^0$, defined as

$$(3.16) \quad \tilde{\mathcal{T}}\hat{\phi} = \hat{\phi} - \hat{\phi}_0\lambda_0^- - \hat{\phi}_{n_-}\lambda_{n_-}^- + \hat{\phi}_0 \sum_{i=1}^r \gamma_i^{1d} \lambda_i^- + \hat{\phi}_{n_-} \sum_{i=n_- - r}^{n_- - 1} \gamma_i^{1d} \lambda_i^-,$$

where $\hat{\phi} \in \mathbb{V}_-^0$. Indeed, this correction accounts for the polynomial moments: For $\hat{\phi}^- \in \mathbb{V}_-^0$ and $q \in \mathbb{Q}_{r-1}[\hat{x}]$, we observe

$$\int \tilde{\mathcal{T}}\hat{\phi}q = \int \hat{\phi}q,$$

by the definition of the correction coefficients γ^{1d} . Hence, we finally set

$$(3.17) \quad \mathcal{R}_0 = \tilde{\mathcal{T}}\tilde{\mathcal{R}}.$$

The moment preservation of the full restriction operator \mathcal{R} in (3.13) is now apparent: Observe for $\hat{\phi} \in \hat{V}_+^0$ that

$$\begin{aligned} \int (\mathcal{R}\hat{\phi})q_j &= \int \left((\text{id} - \mathcal{T})\hat{\phi} + \mathcal{R}_0\mathcal{T}\hat{\phi} \right) q_j \\ &= \int \left((\text{id} - \mathcal{T})\hat{\phi} + \tilde{\mathcal{T}}\tilde{\mathcal{R}}\mathcal{T}\hat{\phi} \right) q_j \\ &= \int \left((\text{id} - \mathcal{T})\hat{\phi} + \tilde{\mathcal{R}}\mathcal{T}\hat{\phi} \right) q_j \\ &= \int \left((\text{id} - \mathcal{T})\hat{\phi} + \mathcal{T}\hat{\phi} \right) q_j \\ &= \int \hat{\phi}q_j, \quad \forall j, \end{aligned}$$

where we used the moment preservation of $\tilde{\mathcal{T}}$ and $\tilde{\mathcal{R}}$. And by construction (3.12) also holds.

Note that this indeed defines a projection: Let $\hat{\phi} \in \mathbb{V}_-^0 \subset \mathbb{V}_+^0$, then

$$\mathcal{T}\hat{\phi} = \hat{\phi} - \hat{\phi}_0\lambda_0^- - \hat{\phi}_{n_+}\lambda_{n_+}^- \in \mathbb{V}_{-,0}^0,$$

thus $\mathcal{R}_0\mathcal{T}\hat{\phi} = \mathcal{T}\hat{\phi}$ by definition of the L^2 -projection and $\tilde{\mathcal{T}}$, hence

$$\mathcal{R}\hat{\phi} = \hat{\phi}_0\lambda_0^- + \hat{\phi}_{n_+}\lambda_{n_+}^- + \mathcal{T}\hat{\phi} = \hat{\phi}.$$

To summarize, we constructed the restriction operator

$$\mathcal{R} : \mathbb{V}_+^0 \rightarrow \mathbb{V}_-^0, \hat{\phi} \mapsto \mathcal{R}\hat{\phi} = \hat{\phi}_0\lambda_0^- + \hat{\phi}_{n_+}\lambda_{n_+}^- + \tilde{\mathcal{T}}\tilde{\mathcal{R}}\mathcal{T}\hat{\phi},$$

consisting of the two truncation operators \mathcal{T} defined in equation (3.14) and $\tilde{\mathcal{T}}$ defined in equation (3.16) and the L^2 -projection $\tilde{\mathcal{R}}$ from equation (3.15). This operator is a projection on the univariate logical edge-parallel space \mathbb{V}_-^0 that preserves the vertex degrees of freedom and is preserving polynomial moments up to order r .

The description of its matrix \mathbf{R} and its detailed construction is given in the Section B.2.

Local edge conforming projection. We introduce the averaged basis function perpendicular to the edge e :

$$(3.18) \quad \bar{\lambda}_\perp^e = \frac{1}{2} \left(\lambda_{\perp,0}^- + \lambda_{\perp,0}^+ \right),$$

which uses the parametrization in (3.9) and makes the following definitions more readable. Mapping a coarse basis function to the fine space, we have to consider the following cases, where only the ones with support on the interface and not on the vertex are affected:

$$P_e : \Lambda_j^- \mapsto \begin{cases} \mathcal{F}^0(\lambda_{j_1}^- \otimes \bar{\lambda}_\perp^e) & \text{if } 0 < j_1 < n_-, j_2 = 0, \\ \Lambda_j^- & \text{else,} \end{cases}$$

note that this is well-defined since $\hat{V}_\parallel^{0,-} \subset \hat{V}_\parallel^{0,+}$. (We omit the explicit application of the extension operator here) For fine basis functions, we need to additionally apply the restriction operator in the parallel direction:

$$P_e : \Lambda_j^+ \mapsto \begin{cases} \mathcal{F}^0(\mathcal{R}\lambda_{j_1}^+ \otimes \bar{\lambda}_\perp^e) & \text{if } 0 < j_1 < n_+, j_2 = 0, \\ \Lambda_j^+ & \text{else.} \end{cases}$$

Preservation of polynomial moments. Again, following Definition 2.5 as in Section 3.1, we add (interior) correction terms from both sides in the perpendicular direction of the interface, which are independent of the patch as explained in Remark 3.4. As for the vertex-conforming projection, we have to map coarse and fine basis functions on the edge, namely $\Lambda_{(i,0)}^-$ and $\Lambda_{(i,0)}^+$, pulling them back to the logical domain from both of the tensor-product patches, namely Ω_- and Ω_+ , and checking for the moment preservation.

Since we want to preserve vertex degrees of freedom, we only consider $0 < i < n_\pm$ for now. Starting with a coarse basis function, the ansatz reads

$$P_e \Lambda_{(i,0)}^- = \mathcal{F}^0 \left(\lambda_i^- \otimes \left(\bar{\lambda}_\perp^e + \sum_{m=1}^r a_m \lambda_{\perp,m}^- + \sum_{m=1}^r \tilde{a}_m \lambda_{\perp,m}^+ \right) \right).$$

Thus, the condition for the coarse patch Ω_- , where the pullbacks are given by

$$(\mathcal{F}^0)^{-1}(P_e \Lambda_{(i,0)}^-|_{\Omega_-}) = \lambda_i^- \otimes \left(\frac{1}{2} \lambda_0^- + \sum_{m=1}^r a_m \lambda_{\perp,m}^- \right), \quad (\mathcal{F}^0)^{-1}(\Lambda_{(i,0)}^-|_{\Omega_-}) = \lambda_i^- \otimes \lambda_{\perp,0}^-,$$

reads

$$\begin{aligned} \int_{\hat{\Omega}_-} \left(\lambda_i^- \otimes \left(\frac{1}{2} \lambda_{\perp,0}^- + \sum_{m=1}^r a_m \lambda_{\perp,m}^- \right) \right) q_j &= \int_{\hat{\Omega}_-} \lambda_i^- \otimes \lambda_{\perp,0}^- q_j \\ \Leftrightarrow \sum_{m=1}^r a_m \int_{\hat{\Omega}_-} \lambda_i^- \otimes \lambda_{\perp,m}^- q_j &= \frac{1}{2} \int_{\hat{\Omega}_-} \lambda_i^- \otimes \lambda_{\perp,0}^- q_j. \end{aligned}$$

On the fine patch Ω_+ , the pullbacks are given by

$$(\mathcal{F}^0)^{-1}(P_e \Lambda_{(i,0)}^-|_{\Omega_+}) = \lambda_i^- \otimes \left(\frac{1}{2} \lambda_{\perp,0}^+ + \sum_{m=1}^r \tilde{a}_m \lambda_{\perp,m}^+ \right), \quad (\mathcal{F}^0)^{-1}(\Lambda_{(i,0)}^-|_{\Omega_+}) = 0,$$

and the ansatz reads

$$\begin{aligned} \int_{\hat{\Omega}_+} \left(\mathcal{E} \lambda_i^- \otimes \left(\frac{1}{2} \lambda_{\perp,0}^+ + \sum_{m=1}^r \tilde{a}_m \lambda_{\perp,m}^+ \right) \right) q_j &= 0 \\ \Leftrightarrow \sum_{m=1}^r \tilde{a}_m \int_{\hat{\Omega}_+} \mathcal{E} \lambda_i^- \otimes \lambda_{\perp,m}^+ q_j &= -\frac{1}{2} \int_{\hat{\Omega}_+} \mathcal{E} \lambda_i^- \otimes \frac{1}{2} \lambda_{\perp,0}^+ q_j. \end{aligned}$$

We realize that the parallel-component of the integrals is equal (thus moment-preserving), so there is no need for correction. The coefficients along the perpendicular direction are given with an analogous formula as in the vertex case, i.e. (3.7), where the assumed orientation in this section does not change the integrals. Thus, we have

$$\mathbf{a} = \frac{1}{2} \gamma^{1d}, \quad \tilde{\mathbf{a}} = -\frac{1}{2} \gamma^{1d}.$$

Introducing the patch-wise correction term \mathbf{C}^e as

$$(3.19) \quad \mathbf{C}^e = \frac{1}{2} \sum_{m=1}^r \gamma_m^{1d} \left(\lambda_{\perp,m}^- - \lambda_{\perp,m}^+ \right),$$

we are able to define the moment-preserving vertex-conforming operator P_e for coarse edge-interior basis functions by

$$P_e \Lambda_{(i,0)}^- = \mathcal{F}^0 \left(\lambda_i^- \otimes (\bar{\lambda}_{\perp}^e + \mathbf{C}^e) \right).$$

Next, we want to do the same derivation for fine basis function. If we write the projection ansatz for a fine basis function, we get:

$$P_e \Lambda_{(i,0)}^+ = \mathcal{F}^0 \left(\mathcal{R} \lambda_i^+ \otimes \left(\bar{\lambda}_{\perp}^e + \sum_{m=1}^r a_m \lambda_{\perp,m}^+ + \sum_{m=1}^r \tilde{a}_m \lambda_{\perp,m}^- \right) \right).$$

On the coarse patch Ω_- , the pullbacks read

$$(\mathcal{F}^0)^{-1}(P_e \Lambda_{(i,0)}^+|_{\Omega_-}) = \mathcal{R} \lambda_i^+ \otimes \left(\frac{1}{2} \lambda_{\perp,0}^- + \sum_{m=1}^r \tilde{a}_m \lambda_{\perp,m}^- \right), \quad (\mathcal{F}^0)^{-1}(\Lambda_{(i,0)}^+|_{\Omega_-}) = 0,$$

which amounts to

$$\begin{aligned} \int_{\hat{\Omega}_-} \left(\mathcal{R} \lambda_i^+ \otimes \left(\frac{1}{2} \lambda_{\perp,0}^- + \sum_{m=1}^r \tilde{a}_m \lambda_{\perp,m}^- \right) \right) q_j &= 0 \\ \Leftrightarrow \sum_{m=1}^r \tilde{a}_m \int_{\hat{\Omega}_-} \mathcal{R} \lambda_i^+ \otimes \lambda_{\perp,m}^- q_j &= -\frac{1}{2} \int_{\hat{\Omega}_-} \mathcal{R} \lambda_i^+ \otimes \lambda_{\perp,0}^- q_j, \end{aligned}$$

whereas before, the parallel-component cancels leading to only one-dimensional correction terms in perpendicular direction. On the other hand, on the fine patch Ω_+ we have the pullbacks

$$\begin{aligned} (\mathcal{F}^0)^{-1}(P_e \Lambda_{(i,0)}^+|_{\Omega_+}) &= \mathcal{R} \lambda_i^+ \otimes \left(\frac{1}{2} \lambda_{\perp,0}^+ + \sum_{m=1}^r a_m \lambda_{\perp,m}^+ \right), \\ (\mathcal{F}^0)^{-1}(\Lambda_{(i,0)}^+|_{\Omega_+}) &= \lambda_i^+ \otimes \lambda_{\perp,0}^+, \end{aligned}$$

and get for the ansatz:

$$\begin{aligned} \int_{\hat{\Omega}_+} \left(\mathcal{R}\lambda_i^+ \otimes \left(\frac{1}{2}\lambda_{\perp,0}^+ + \sum_{m=1}^r a_m \lambda_{\perp,m}^+ \right) \right) q_j &= \int_{\hat{\Omega}_+} \lambda_i^+ \otimes \lambda_{\perp,0}^+ q_j \\ \Leftrightarrow \sum_{m=1}^r a_m \int_{\hat{\Omega}_+} \mathcal{R}\lambda_i^+ \otimes \lambda_{\perp,m}^+ q_j &= \int_{\hat{\Omega}_+} \left(\lambda_i^+ - \frac{1}{2}\mathcal{R}\lambda_i^+ \right) \otimes \lambda_{\perp,0}^+ q_j. \end{aligned}$$

Here, we require moment-preservation of the restriction \mathcal{R} operator, as was derived in Section 3.2, which allows for the parallel-component to cancel out just as before. This allows us to conclude with the same correction term defined in (3.19) and define the moment preserving edge-conforming operator for fine basis functions as

$$P_e \Lambda_{(i,0)}^+ = \mathcal{F}^0 \left(\mathcal{R}\lambda_i^+ \otimes (\bar{\lambda}_{\perp}^e - \mathbf{c}^e) \right).$$

For now, we did not consider the vertex basis functions (on the edge) in the same way as the current ansatz would change the degree of freedom at the vertex. In order to also preserve moments across the edge for these basis functions, we have to add another correction term, where the idea is to consider a linear combination of logical basis functions in parallel direction that are supported on the edge, but not on the vertex, such that it has the same moments as the vertex basis function: Assume the vertex v is one of the two vertices on the edge e at (basis function) index $\mathbf{0}$ on both patches and define a fine spline $\mu_v^+ \in \mathbb{V}_+^0$ in parallel coordinate such that $\mu_v^+(v_{\parallel}) = 0$ and

$$\int_0^1 \mu_v^+ q = \int_0^1 \lambda_0^+ q, \quad \forall q \in \mathbb{Q}_{r-1}[\hat{x}],$$

holds. This, again, leads to defining

$$(3.20) \quad \mu_v^+ = \sum_{m=1}^r \gamma_m^{1d} \lambda_m^+.$$

In the following proposition, we derive the existence and explicit form of an analogous coarse spline μ_v^- and the definition of the edge-based projection for the vertex basis functions of both patches:

Proposition 3.7. There exists a coarse spline $\mu_v^- \in \mathbb{V}_-^0$, such that defining the projection of the vertex basis functions from each patch as

$$P_e \Lambda_{\mathbf{0}}^+ = \mathcal{F}^0 \left(\mathcal{R}\lambda_0^+ \otimes \bar{\lambda}_{\perp}^e - \mathcal{R}\mu_v^+ \otimes \mathbf{c}^e \right),$$

where μ_v^+ is defined in (3.20), and

$$P_e \Lambda_{\mathbf{0}}^- = \mathcal{F}^0 \left(\lambda_0^- \otimes \bar{\lambda}_{\perp}^e + \mu_v^- \otimes \mathbf{c}^e \right),$$

where μ_v^- is derived in (3.21), preserves polynomial moments up to order r and preserves continuity at the vertex.

Proof. In order to derive the form of μ_v^- , we consider the vertex-continuous function $\phi \in V_h^0$ defined as

$$(\mathcal{F}^0)^{-1}(\phi) = \lambda_0^- \otimes \lambda_{\perp,0}^- + \mathcal{E}\lambda_0^- \otimes \lambda_{\perp,0}^+ = \lambda_0^- \otimes \left(\lambda_{\perp,0}^- + \lambda_{\perp,0}^+ \right) = \lambda_0^- \otimes 2\bar{\lambda}_{\perp}^e,$$

which is supported on the vertex v and should stay unchanged under the projection. To make things more explicit, we use the matrix notation of the extension operator in the following. Looking at ϕ on the fine patch, we observe the relation

$$\mathcal{E}\lambda_0^- \otimes \lambda_{\perp,0}^+ = \sum_{i=0}^{n_+} \mathbf{E}_{i,0} \lambda_i^+ \otimes \lambda_{\perp,0}^+ = \lambda_0^+ \otimes \lambda_{\perp,0}^+ + \sum_{i=1}^{n_+} \mathbf{E}_{i,0} \lambda_i^+ \otimes \lambda_{\perp,0}^+,$$

where the projection of the later part reads

$$\begin{aligned} & (\mathcal{F}^0)^{-1} \left(P_e \mathcal{F}^0 \left(\sum_{i=1}^{n_+} \mathbf{E}_{i,0} \lambda_i^+ \otimes \lambda_{\perp,0}^+ \right) \right) \\ &= \sum_{i=1}^{n_+} \mathbf{E}_{i,0} \mathcal{R} \lambda_i^+ \otimes (\bar{\lambda}_{\perp}^e - \mathbf{C}^e) \\ &= \underbrace{\mathcal{R} \mathcal{E}}_{=\text{id}} \lambda_0^- \otimes (\bar{\lambda}_{\perp}^e - \mathbf{C}^e) - \mathcal{R} \lambda_0^+ \otimes (\bar{\lambda}_{\perp}^e - \mathbf{C}^e). \end{aligned}$$

Thus, we can calculate the full projection $P_e \phi$:

$$\begin{aligned} (\mathcal{F}^0)^{-1}(P_e \phi) &= \lambda_0^- \otimes \bar{\lambda}_{\perp}^e + \mu_v^- \otimes \mathbf{C}^e \\ &\quad + \mathcal{R} \lambda_0^+ \otimes \bar{\lambda}_{\perp}^e - \mathcal{R} \mu_v^+ \otimes \mathbf{C}^e \\ &\quad + \lambda_0^- \otimes (\bar{\lambda}_{\perp}^e - \mathbf{C}^e) \\ &\quad - \mathcal{R} \lambda_0^+ \otimes (\bar{\lambda}_{\perp}^e - \mathbf{C}^e) \\ &= \lambda_0^- \otimes 2\bar{\lambda}_{\perp}^e \\ &\quad + (\mu_v^- - \mathcal{R} \mu_v^+ - \lambda_0^- + \mathcal{R} \lambda_0^+) \otimes \mathbf{C}^e. \end{aligned}$$

Subtracting the original function ϕ then leads to the condition

$$0 = P_e \phi - \phi = \mathcal{F}^0 \left((\mu_v^- - \mathcal{R} \mu_v^+ - \lambda_0^- + \mathcal{R} \lambda_0^+) \otimes \mathbf{C}^e \right),$$

where we conclude with defining μ_v^- as

$$(3.21) \quad \mu_v^- = \lambda_0^- + \mathcal{R} (\mu_v^+ - \lambda_0^+),$$

as the edge conforming projection P_e should leave ϕ unchanged.

Indeed, since $\mu_v^{\pm}(v) = 0$, we preserve continuity: Let $\phi = \sum_k \sum_{\mathbf{i}} \phi_{\mathbf{i}}^k \Lambda_{\mathbf{i}}^k \in V_{\text{pw}}^0$ be continuous at the vertex v , then

$$(P_e \phi)|_{\Omega_{\pm}}(v) = \sum_{k=\pm} \phi_0(P_e \Lambda_0^k)|_{\Omega_{\pm}}(v) = \phi_0 \mathcal{F}^0 (\mathcal{R} \lambda_0^+ \otimes \bar{\lambda}_{\perp}^e + \lambda_0^- \otimes \bar{\lambda}_{\perp}^e) |_{\Omega_{\pm}}(v) = \phi_0.$$

The preservation of polynomial moments comes from the ansatz as before and from the fact that μ_v^+ is constructed to preserve the moments of λ_0^+ , which directly transfers to μ_v^- preserving the moments of λ_0^- . \square

Of course this construction holds similarly for the second vertex on the edge e . Finally, we are in the position to give the following definition

Definition 3.8. The local edge conforming projection $P_e : V_{\text{pw}}^0 \rightarrow V_{\text{pw}}^0$ is defined as

$$P_e : \begin{cases} \Lambda_j^- \mapsto \begin{cases} \mathcal{F}^0(\lambda_{j_1}^- \otimes (\bar{\lambda}_\perp^e + \mathbb{C}^e)) & \text{if } 0 < j_1 < n_-, j_2 = 0, \\ \mathcal{F}^0(\lambda_{j_1}^- \otimes \bar{\lambda}_\perp^e + \mu_v^- \otimes \mathbb{C}^e) & \text{if } j_1 \in \{0, n_-\}, j_2 = 0, \text{ for } v \text{ at } \mathbf{j}, \\ \Lambda_j^- & \text{else,} \end{cases} \\ \Lambda_j^+ \mapsto \begin{cases} \mathcal{F}^0(\mathcal{R}\lambda_{j_1}^+ \otimes (\bar{\lambda}_\perp^e - \mathbb{C}^e)) & \text{if } 0 < j_1 < n_-, j_2 = 0, \\ \mathcal{F}^0(\mathcal{R}\lambda_{j_1}^+ \otimes \bar{\lambda}_\perp^e - \mathcal{R}\mu_v^+ \otimes \mathbb{C}^e) & \text{if } j_1 \in \{0, n_+\}, j_2 = 0, \text{ for } v \text{ at } \mathbf{j}, \\ \Lambda_j^+ & \text{else,} \end{cases} \\ \Lambda_j^k \mapsto \Lambda_j^k \quad \text{if } k \neq k^-, k^+, \end{cases}$$

where v denotes the vertex corresponding to the index \mathbf{j} in both intermediate cases, λ_j^k are the scalar patch-wise basis functions defined in (2.12), $\bar{\lambda}_\perp^e$ the edge-conforming spline in (3.18), \mathbb{C}^e the patch-wise correction term in (3.19), μ_v^- and μ_v^+ the vertex correction terms in (3.21) and (3.20), and the restriction operator \mathcal{R} in (3.11). On other patches $k \neq k^-, k^+$, it acts as the identity.

Using this definition, we conclude the section with the proof of Proposition 3.2.

Proof of Proposition 3.2.

- (1) In order to show that $P_e\phi$ is continuous on e , let $\phi = \sum_k \sum_{\mathbf{i}} \phi_{\mathbf{i}}^k \Lambda_{\mathbf{i}}^k \in V_{\text{pw}}^0$ be continuous on vertices and $\mathbf{x} = F(\hat{x}_1, 0)$ be a point on the interior of the edge e . Evaluating $P_e\phi$ on e at \mathbf{x} gives

$$\begin{aligned} P_e\phi(\mathbf{x}) &= \sum_{k \in \mathcal{K}(e)} \sum_{\mathbf{i}} \phi_{\mathbf{i}}^k (P_e \Lambda_{\mathbf{i}}^k)(\mathbf{x}) \\ &= \sum_{\mathbf{i}} \phi_{(i,0)}^- \mathcal{F}^0(\lambda_i^- \otimes \bar{\lambda}_\perp^e)(\mathbf{x}) \\ &\quad + \sum_{\mathbf{i}} \phi_{(i,0)}^+ \mathcal{F}^0(\mathcal{R}\lambda_i^+ \otimes \bar{\lambda}_\perp^e)(\mathbf{x}) \\ &= \sum_{\mathbf{i}} \phi_{(i,0)}^- \lambda_i^-(\hat{x}_1) \otimes \frac{1}{2} (1|_{\Omega_-} + 1|_{\Omega_+}) \\ &\quad + \sum_{\mathbf{i}} \phi_{(i,0)}^+ \mathcal{R}\lambda_i^+(\hat{x}_1) \otimes \frac{1}{2} (1|_{\Omega_-} + 1|_{\Omega_+}). \end{aligned}$$

Thus, the projected function is continuous on the edge interior, with values

$$P_e\phi(\mathbf{x}) = \frac{1}{2} \left(\sum_{\mathbf{i}} \phi_{(i,0)}^- \lambda_i^-(\hat{x}_1) + \sum_{\mathbf{i}} \phi_{(i,0)}^+ \mathcal{R}\lambda_i^+(\hat{x}_1) \right).$$

Using the assumption of continuity at the vertices, this continuity extends to the whole edge.

- (2) Next, we want to show: $P_e\phi = \phi$ if and only if ϕ is continuous on e . (with ϕ already continuous on vertices) Again, " \implies " follows from (1). For the other direction, assume $\phi = \sum_k \sum_{\mathbf{i}} \phi_{\mathbf{i}}^k \Lambda_{\mathbf{i}}^k \in V_{\text{pw}}^0$ is continuous on vertices

and the edge e . Being continuous on the full edge means that we can write ϕ on e as

$$\begin{aligned} \sum_{\substack{\mathbf{i} \\ i_2=0}} \phi_{\mathbf{i}}^- \Lambda_{\mathbf{i}}^- &= \sum_{\substack{\mathbf{i} \\ i_2=0}} \phi_{\mathbf{i}}^+ \Lambda_{\mathbf{i}}^+ \\ \iff \sum_{i=0}^{n_-} \phi_{(i,0)}^- \lambda_i^- &= \sum_{i=0}^{n_+} \phi_{(i,0)}^+ \lambda_i^+. \end{aligned}$$

This relation is invariant under the restriction operator, i.e.

$$\begin{aligned} (3.22) \quad \sum_{i=0}^{n_+} \phi_{(i,0)}^+ \mathcal{R} \lambda_i^+ &= \mathcal{R} \sum_{i=0}^{n_+} \phi_{(i,0)}^+ \lambda_i^+ = \mathcal{R} \sum_{i=0}^{n_-} \phi_{(i,0)}^- \lambda_i^- \\ &= \sum_{i=0}^{n_-} \phi_{(i,0)}^- \lambda_i^- = \sum_{i=0}^{n_+} \phi_{(i,0)}^+ \lambda_i^+, \end{aligned}$$

and also allows us to write the edge terms

$$(3.23) \quad \sum_{i=0}^{n_{\pm}} \phi_{(i,0)}^{\pm} \lambda_i^{\pm} \otimes \bar{\lambda}_{\perp}^e = \frac{1}{2} \sum_{i=0}^{n_-} \phi_{(i,0)}^- \lambda_i^- \otimes \lambda_{\perp,0}^- + \frac{1}{2} \sum_{i=0}^{n_+} \phi_{(i,0)}^+ \lambda_i^+ \otimes \lambda_{\perp,0}^+.$$

The projection of ϕ can be written as

$$\begin{aligned} (\mathcal{F}^0)^{-1} (P_e \phi) &= \sum_{k \in \mathcal{K}(e)} \sum_{\mathbf{i}} \phi_{\mathbf{i}}^k (\mathcal{F}^0)^{-1} (P_e \Lambda_{\mathbf{i}}^k) \\ &= \sum_{k \in \mathcal{K}(e)} \sum_{\substack{\mathbf{i} \\ i_2 \neq 0}} \phi_{\mathbf{i}}^k (\mathcal{F}^0)^{-1} (P_e \Lambda_{\mathbf{i}}^k) \\ &\quad + \sum_{\substack{\mathbf{i} \\ 0 < i_1 < n_k, i_2=0}} \phi_{\mathbf{i}}^k (\mathcal{F}^0)^{-1} (P_e \Lambda_{\mathbf{i}}^k) \\ &\quad + \sum_{i_1=0, n_k, i_2=0} \phi_{\mathbf{i}}^k (\mathcal{F}^0)^{-1} (P_e \Lambda_{\mathbf{i}}^k), \end{aligned}$$

where we separated the indices to interior, edge and vertex terms. Writing out the projections explicitly, we get

$$\begin{aligned} (\mathcal{F}^0)^{-1} (P_e \phi) &= \sum_{k \in \pm} \sum_{\substack{\mathbf{i} \\ i_2 \neq 0}} \phi_{\mathbf{i}}^k \lambda_{i_1}^k \otimes \lambda_{\perp, i_2}^k \\ &\quad + \sum_{i=1}^{n_- - 1} \phi_{(i,0)}^- \lambda_i^- \otimes \bar{\lambda}_{\perp}^e + \phi_{(i,0)}^- \lambda_i^- \otimes \mathbf{C}^e \\ &\quad + \sum_{i=1}^{n_+ - 1} \phi_{(i,0)}^+ \mathcal{R} \lambda_i^+ \otimes \bar{\lambda}_{\perp}^e + \phi_{(i,0)}^+ \mathcal{R} \lambda_i^+ \otimes -\mathbf{C}^e \\ &\quad + \sum_{i=0, n_-} \phi_{(i,0)}^- \lambda_i^- \otimes \bar{\lambda}_{\perp}^e + \phi_{(i,0)}^- \mu_{v(i)}^- \otimes \mathbf{C}^e \\ &\quad + \sum_{i=0, n_+} \phi_{(i,0)}^+ \mathcal{R} \lambda_i^+ \otimes \bar{\lambda}_{\perp}^e + \phi_{(i,0)}^+ \mathcal{R} \mu_{v(i)}^+ \otimes -\mathbf{C}^e. \end{aligned}$$

After adding-subtracting vertex terms and regrouping, it reads

$$\begin{aligned}
(\mathcal{F}^0)^{-1}(P_e \phi) &= \sum_{k \in \pm} \sum_{\substack{\mathbf{i} \\ i_2 \neq 0}} \phi_{\mathbf{i}}^k \lambda_{i_1}^k \otimes \lambda_{\perp, i_2}^k \\
&\quad + \sum_{i=0}^{n_-} \phi_{(i,0)}^- \lambda_i^- \otimes \bar{\lambda}_{\perp}^e + \sum_{i=0}^{n_+} \phi_{(i,0)}^+ \mathcal{R} \lambda_i^+ \otimes \bar{\lambda}_{\perp}^e \\
&\quad + \sum_{i=0}^{n_-} \phi_{(i,0)}^- \lambda_i^- \otimes \mathbf{C}^e + \sum_{i=0}^{n_+} \phi_{(i,0)}^+ \mathcal{R} \lambda_i^+ \otimes -\mathbf{C}^e \\
&\quad - \sum_{i=0, n_-} \phi_{(i,0)}^- \lambda_i^- \otimes \mathbf{C}^e - \sum_{i=0, n_+} \phi_{(i,0)}^+ \mathcal{R} \lambda_i^+ \otimes -\mathbf{C}^e \\
&\quad + \sum_{i=0, n_-} \phi_{(i,0)}^- \mu_{v(i)}^- \otimes \mathbf{C}^e + \sum_{i=0, n_+} \phi_{(i,0)}^+ \mathcal{R} \mu_{v(i)}^+ \otimes -\mathbf{C}^e,
\end{aligned}$$

and we apply the relation (3.23) to the second line in order to recover ϕ , and apply the relation (3.22) to the third line to cancel out. Finally, we use the continuity at the vertices to write

$$\begin{aligned}
(\mathcal{F}^0)^{-1}(P_e \phi) &= \sum_{k \in \pm} \sum_{\mathbf{i}} \phi_{\mathbf{i}}^k \lambda_{i_1}^k \otimes \lambda_{\perp, i_2}^k \\
&\quad + \sum_{i=0}^{n_-} \phi_{(i,0)}^- \lambda_i^- \otimes \mathbf{C}^e - \sum_{i=0}^{n_-} \phi_{(i,0)}^- \lambda_i^- \otimes \mathbf{C}^e \\
&\quad + \sum_{i=0, n_{\pm}} \phi(v(i)) \left(-\lambda_i^- + \mu_{v(i)}^- + \mathcal{R} \lambda_i^+ - \mathcal{R} \mu_{v(i)}^+ \right) \otimes \mathbf{C}^e \\
&= (\mathcal{F}^0)^{-1}(\phi),
\end{aligned}$$

where the definition of $\mu_{\mathbf{v}}^-$ from Proposition 3.7 is used in the last step. Thus, we showed $P_e \phi = \phi$. Note that we wrote $v(i)$, with $i = 0, n_{\pm}$, to denote the vertex on the edge e with associated index $(i, 0)$.

- (3) The preservation of polynomial moments holds by construction in Section 3.2.
- (4) The edge-based operators for different edges are commuting since the interiors of all edges are disjoint, the projection P_e only acts on basis functions in the edge interior of e by construction, leaving the rest of the basis functions unchanged. The assumed continuity at vertices yields result.

□

4. CONFORMING PROJECTION OPERATORS ON V_{pw}^1

In this section we construct a conforming projection

$$\mathbf{P}^1 : V_{\text{pw}}^1 \rightarrow V_{\text{pw}}^1,$$

onto the space $V_h^1 = V_{\text{pw}}^1 \cap H(\text{curl}; \Omega)$. Here the curl-conformity amounts to a tangential continuity constraint. For simplicity of the presentation, we make the same assumptions on the geometry of the patches as in Section 3.2, and consider the logical domain $\hat{\Omega}(\mathbf{e})$ around an horizontal edge $\hat{\mathbf{e}}$ corresponding to the logical patches $\hat{\Omega}_{\pm}$ associated with the parametrization $F = F(\mathbf{e}) : \hat{\Omega}(\mathbf{e}) \rightarrow \Omega(\mathbf{e})$, see Figure 1. On every patch, the logical spaces are of the form

$$\hat{V}_k^1 = \begin{pmatrix} \mathbb{W}_k^1 \otimes \mathbb{W}_k^0 \\ \mathbb{W}_k^0 \otimes \mathbb{W}_k^1 \end{pmatrix},$$

therefore the univariate function spaces along the edge $\hat{\mathbf{e}}$, are given by $(\hat{V}_{\pm}^1 \cdot \hat{\boldsymbol{\tau}}_{\mathbf{e}})_{\parallel} = \mathbb{W}_{\pm}^1$, which is the parallel (horizontal) direction of the first component of the logical space \hat{V}_{\pm}^1 . The corresponding component of the projected fields must then be continuous across the edge $\hat{\mathbf{e}}$, that is in the edge-perpendicular direction.

Hence, in Section 4.1, we extend the prior introduced extension \mathcal{E} and restriction operators \mathcal{R} (which are applied in the edge-parallel coordinate) to the space \mathbb{W}_{\pm}^1 . The averaging and moment corrections are still done in the edge-perpendicular direction (hence on \mathbb{W}_{\pm}^0) and thus allow to reuse prior definitions like the correction terms γ^{1d} in (3.7).

In Definition 4.3 below, we will define a logical scalar edge-based operator $\hat{P}_{\mathbf{e}}^1$ acting on a single component of \hat{V}_{pw}^1 depending on the orientation of the edge \mathbf{e} . Since we assumed \mathbf{e} to be horizontal, the vector-valued edge-based operator $\mathbf{P}_{\mathbf{e}}^1$ takes the form

$$(4.1) \quad \mathbf{P}_{\mathbf{e}}^1 \mathbf{u} = \mathcal{F}^1 \begin{pmatrix} \hat{P}_{\mathbf{e}}^1 \hat{u}_1 \\ \hat{u}_2 \end{pmatrix},$$

where $\hat{\mathbf{u}} = (\mathcal{F}^1)^{-1}(\mathbf{u}) \in \hat{V}_{\text{pw}}^1$, $\mathbf{u} \in V_{\text{pw}}^1$. Our construction will satisfy the following properties.

Proposition 4.1. Given $\mathbf{e} \in \mathcal{E}$ with tangential vector $\boldsymbol{\tau}_{\mathbf{e}}$, let $\mathbf{P}_{\mathbf{e}}^1 : V_{\text{pw}}^1 \rightarrow V_{\text{pw}}^1$ be the edge-conforming projection (4.1) associated with the logical operator $\hat{P}_{\mathbf{e}}^1$ from Definition 4.3 below, with an order of moment preservation $r = r(\mathbf{P}^1)$ such that $0 \leq r \leq p$. Then the following properties hold for all $\mathbf{u} \in V_{\text{pw}}^1$:

- (1) $\mathbf{P}_{\mathbf{e}}^1 \mathbf{u} \cdot \boldsymbol{\tau}_{\mathbf{e}}$ is continuous across \mathbf{e} .
- (2) $\mathbf{P}_{\mathbf{e}}^1 \mathbf{u} = \mathbf{u}$ if and only if $\mathbf{u} \cdot \boldsymbol{\tau}_{\mathbf{e}}$ is continuous.
- (3) $\mathbf{P}_{\mathbf{e}}^1$ preserves polynomial moments of order r .
- (4) $\mathbf{P}_{\mathbf{e}}^1 \mathbf{P}_{\mathbf{e}'}^1 \mathbf{u} = \mathbf{P}_{\mathbf{e}'}^1 \mathbf{P}_{\mathbf{e}}^1 \mathbf{u}$ for any $\mathbf{e}' \in \mathcal{E}$.

The proof will be given in Section 4.1. This leads to the definition of the conforming projection operator of V_h^1 .

Theorem 4.2. *The operator*

$$(4.2) \quad \mathbf{P}^1 = \prod_{\mathbf{e} \in \mathcal{E}} \mathbf{P}_{\mathbf{e}}^1 : V_{\text{pw}}^1 \rightarrow V_{\text{pw}}^1,$$

involving the r -th order moment-preserving edge-conforming projection as in Proposition 4.1, is an r -th order moment-preserving projection onto the conforming subspace V_h^1 .

Proof. Note that (4.2) is well-defined, as the order of the products does not matter thanks to (4) in Proposition 4.1. For the range property of \mathbf{P}^1 , let $\mathbf{u} \in V_{\text{pw}}^1$: $\mathbf{P}^1 \mathbf{u}$ is continuous along any edge by (1) in Proposition 4.1. Thus, \mathbf{P}^1 maps into the continuous space V_h^1 . The projection property directly follows from (2) in Proposition 4.1. Again, the moment preservation holds by (3) in Proposition 4.1. \square

4.1. Edge-based projections. We fix an edge $e \in \mathcal{E}$ and use a similar notation to Section 3.2 applied to the derived spaces \hat{V}_\pm^1 . As discussed before, the continuity constraint is now only enforced along the tangential vector $\boldsymbol{\tau}_e$, i.e. in the space $(\hat{V}_\pm^1 \cdot \hat{\boldsymbol{\tau}}_e)_\parallel = \mathbb{W}_\pm^1$.

Extension-restriction operators. Since the edge-local derived spaces are still nested, the extension operator on \mathbb{W}_\pm^1 , i.e.

$$(4.3) \quad \mathcal{E}^1 : \mathbb{W}_-^1 \subset \mathbb{W}_+^1 \longrightarrow \mathbb{W}_+^1$$

is defined completely analogous to Section 3.2.

The restriction is now simpler, as we do not have to preserve vertex conformity but have it automatically through the edge corrections. Thus, the restriction operator

$$(4.4) \quad \mathcal{R}^1 : \mathbb{W}_+^1 \longrightarrow \mathbb{W}_-^1 \subset \mathbb{W}_+^1,$$

now is simply defined as the L^2 -projection from the fine space \mathbb{W}_+^1 onto the coarse space \mathbb{W}_-^1 , i.e.

$$(4.5) \quad \int \lambda_j^{1,-} \mathcal{R}^1 \lambda_i^{1,+} = \int \lambda_j^{1,-} \lambda_i^{1,+}, \quad \forall j = 0, \dots, n_- - 1, i = 0, \dots, n_+ - 1.$$

This operator is well-defined and moment preserving of order p , again by the same argument that \mathbb{W}_-^1 contains polynomials up to degree $p - 1$.

Again, the construction of the matrix forms \mathbf{E}^1 and \mathbf{R}^1 are presented in detail in the Section B.3.

Local edge conforming projection. Using the same edge-averaging function, that is defined in the edge-perpendicular direction in the same logical space as in the V^0 case, namely (3.18), we can directly define the local edge-based projection without any moment preservation as

$$\hat{P}_e^1 : \begin{cases} \lambda_{j_1}^{1,-} \otimes \lambda_{\perp,j_2}^- \mapsto \begin{cases} \lambda_{j_1}^{1,-} \otimes \bar{\lambda}_\perp^e & \text{if } j_2 = 0, \\ \lambda_{j_1}^{1,-} \otimes \lambda_{\perp,j_2}^- & \text{else.} \end{cases} \\ \lambda_{j_1}^{1,+} \otimes \lambda_{\perp,j_2}^+ \mapsto \begin{cases} \mathcal{R}^1 \lambda_{j_1}^{1,+} \otimes \bar{\lambda}_\perp^e & \text{if } j_2 = 0, \\ \lambda_{j_1}^{1,+} \otimes \lambda_{\perp,j_2}^+ & \text{else.} \end{cases} \end{cases}$$

Preservation of polynomial moments. Similar to Section 3.2, we can write out the derivation of the moment preservation for the edge-based projection \hat{P}_e^1 following Definition 2.5. Since \mathcal{R}^1 is moment preserving, the correction terms are only in the edge-perpendicular direction, which is the same logical space $(\hat{V}_\pm^1 \cdot \hat{\tau}_e)_\perp = \mathbb{V}_\pm^0$ as in the V^0 case, we thus arrive at an analogous definition with similar correction coefficients:

Definition 4.3. The logical scalar edge-conforming projection $\hat{P}_e^1 : (\hat{V}_{pw}^1)_1 \rightarrow (\hat{V}_{pw}^1)_1$ is defined as

$$\hat{P}_e^1 : \begin{cases} \lambda_{j_1}^{1,-} \otimes \lambda_{\perp,j_2}^- \mapsto \begin{cases} \lambda_{j_1}^{1,-} \otimes (\bar{\lambda}_\perp^e + \mathbb{C}^e) & \text{if } j_2 = 0, \\ \lambda_{j_1}^{1,-} \otimes \lambda_{\perp,j_2}^- & \text{else} \end{cases} \\ \lambda_{j_1}^{1,+} \otimes \lambda_{\perp,j_2}^+ \mapsto \begin{cases} \mathcal{R}^1 \lambda_{j_1}^{1,+} \otimes (\bar{\lambda}_\perp^e - \mathbb{C}^e) & \text{if } j_2 = 0, \\ \lambda_{j_1}^{1,+} \otimes \lambda_{\perp,j_2}^+ & \text{else} \end{cases} \end{cases},$$

where $\lambda_j^{1,k}$ are the derived scalar patch-wise basis functions from (2.11), $\bar{\lambda}_\perp^e$ the edge-conforming spline in (3.18), \mathbb{C}^e the patch-wise correction term in (3.19), and the restriction operator \mathcal{R}^1 in (4.4). On other patches $k \neq k^-, k^+$, it acts as the identity.

The full edge conforming operator \mathbf{P}_e^1 is then defined as in equation (4.1), and we are able to show its properties.

Proof of Proposition 4.1.

Since we fixed an edge e that is aligned with the first coordinate, its tangent vector is given by $\tau_e = (1 \ 0)^T$.

- (1) To show that $\mathbf{P}_e^1 \mathbf{u} \cdot \tau_e$ is continuous across e , let $\mathbf{u} = \sum_{t=1,2} \sum_k \sum_i \mathbf{u}_{t,i}^k \mathbf{\Lambda}_{t,i}^{1,k} \in V_{pw}^1$ and $\mathbf{x} = F(\hat{x}_1, 0)$ be a point on the edge e .

$$\begin{aligned} (\mathcal{F}^1)^{-1}(\mathbf{P}_e^1 \mathbf{u} \cdot \tau_e)(F^{-1}(\mathbf{x})) &= \sum_{k \in \mathcal{K}(e)} \sum_i \mathbf{u}_{1,i}^k (\hat{P}_e^1(\hat{\Lambda}_{1,i}^{1,k}))_1 (F^{-1}(\mathbf{x})) \\ &= \sum_i \mathbf{u}_{1,i}^- \left(\lambda_{i_1}^{1,-} \otimes \bar{\lambda}_\perp^e \right) (F^{-1}(\mathbf{x})) \\ &\quad + \sum_i \mathbf{u}_{1,i}^+ \left(\mathcal{R}^1 \lambda_{i_1}^{1,+} \otimes \bar{\lambda}_\perp^e \right) (F^{-1}(\mathbf{x})) \\ &= \sum_i \mathbf{u}_{1,i}^- \lambda_{i_1}^-(\hat{x}_1) \otimes \frac{1}{2} (1|_{\Omega_-} + 1|_{\Omega_+}) \\ &\quad + \sum_i \mathbf{u}_{1,i}^+ \mathcal{R} \lambda_{i_1}^+(\hat{x}_1) \otimes \frac{1}{2} (1|_{\Omega_-} + 1|_{\Omega_+}) \end{aligned}$$

Thus the projection is continuous with the same values

$$(\mathcal{F}^1)^{-1}(\mathbf{P}_e^1 \mathbf{u} \cdot \tau_e)(F^{-1}(\mathbf{x})) = \frac{1}{2} \left(\sum_i \mathbf{u}_{1,i}^- \lambda_{i_1}^-(\hat{x}_1) + \sum_i \mathbf{u}_{1,i}^+ \mathcal{R} \lambda_{i_1}^+(\hat{x}_1) \right)$$

coming from both sides of the edge.

- (2) Next, we want to show: $\mathbf{P}_e^1 \mathbf{u} = \mathbf{u}$ if and only if $\mathbf{u} \cdot \tau_e$ is continuous. Again, " \implies " follows from (1). For the other direction, assume $\mathbf{u} \cdot \tau_e$ being continuous on the edge e .

This means that we can write $\mathbf{u} \cdot \boldsymbol{\tau}_e = \mathbf{u}_1$ on e as

$$\sum_{\substack{i_1 \\ i_2=0}} \mathbf{u}_{1,i}^- \Lambda_{1,i}^{1,-} = \sum_{\substack{i_1 \\ i_2=0}} \mathbf{u}_{1,i}^+ \Lambda_{1,i}^{1,+} \iff \sum_{i=0}^{n_- - 1} \mathbf{u}_{1,(i,0)}^- \lambda_i^{1,-} = \sum_{i=0}^{n_+ - 1} \mathbf{u}_{1,(i,0)}^+ \lambda_i^{1,+}.$$

Again, this relation is invariant under the restriction operator, i.e.

$$(4.6) \quad \begin{aligned} \sum_{i=0}^{n_+ - 1} \mathbf{u}_{1,i}^+ \mathcal{R} \lambda_i^{1,+} &= \mathcal{R} \sum_{i=0}^{n_+ - 1} \mathbf{u}_{1,i}^+ \lambda_i^{1,+} = \mathcal{R} \sum_{i=0}^{n_- - 1} \mathbf{u}_{1,i}^- \lambda_i^{1,-} \\ &= \sum_{i=0}^{n_- - 1} \mathbf{u}_{1,i}^- \lambda_i^{1,-} = \sum_{i=0}^{n_+ - 1} \mathbf{u}_{1,i}^+ \lambda_i^{1,+}, \end{aligned}$$

and also allows to decompose the edge functions:

$$(4.7) \quad \sum_{i=0}^{n_{\pm} - 1} \mathbf{u}_{1,(i,0)}^{\pm} \lambda_i^{1,\pm} \otimes \bar{\lambda}_{\perp}^e = \frac{1}{2} \sum_{i=0}^{n_- - 1} \mathbf{u}_{1,(i,0)}^- \lambda_i^{1,-} \otimes \lambda_{\perp,0}^- + \frac{1}{2} \sum_{i=0}^{n_+ - 1} \mathbf{u}_{1,(i,0)}^+ \lambda_i^{1,+} \otimes \lambda_{\perp,0}^+.$$

Using these relations, we can write the projection as

$$\begin{aligned} (\mathcal{F}^1)^{-1}(\mathbf{P}_e^1 \mathbf{u}) &= \sum_{k \in \mathcal{K}(e)} \sum_{\mathbf{i}} \mathbf{u}_{1,i}^k \begin{pmatrix} \hat{P}_e^1(\lambda_{i_1}^{1,k} \otimes \lambda_{\perp,i_2}^k) \\ 0 \end{pmatrix} + \begin{pmatrix} 0 \\ \hat{u}_2 \end{pmatrix} \\ &= \begin{pmatrix} 0 \\ \hat{u}_2 \end{pmatrix} + \sum_{k \in \mathcal{K}(e)} \sum_{\substack{\mathbf{i} \\ i_2 \neq 0}} \mathbf{u}_{1,i}^k \begin{pmatrix} \hat{P}_e^1(\lambda_{i_1}^{1,k} \otimes \lambda_{\perp,i_2}^k) \\ 0 \end{pmatrix} + \sum_{\substack{\mathbf{i} \\ i_2=0}} \mathbf{u}_{1,i}^k \begin{pmatrix} \hat{P}_e^1(\lambda_{i_1}^{1,k} \otimes \lambda_{\perp,i_2}^k) \\ 0 \end{pmatrix} \\ &= \begin{pmatrix} 0 \\ \hat{u}_2 \end{pmatrix} + \sum_{k \in \mathcal{K}(e)} \sum_{\substack{\mathbf{i} \\ i_2 \neq 0}} \mathbf{u}_{1,i}^k \begin{pmatrix} \lambda_{i_1}^{1,k} \otimes \lambda_{\perp,i_2}^k \\ 0 \end{pmatrix} \\ &\quad + \sum_{i=0}^{n_- - 1} \mathbf{u}_{1,(i,0)}^- \begin{pmatrix} \lambda_i^{1,-} \otimes (\bar{\lambda}_{\perp}^e + \mathbf{c}^e) \\ 0 \end{pmatrix} \\ &\quad + \sum_{i=0}^{n_+ - 1} \mathbf{u}_{1,(i,0)}^+ \begin{pmatrix} \mathcal{R}^1 \lambda_i^{1,+} \otimes (\bar{\lambda}_{\perp}^e - \mathbf{c}^e) \\ 0 \end{pmatrix} \\ &= \begin{pmatrix} 0 \\ \hat{u}_2 \end{pmatrix} + \sum_{k \in \mathcal{K}(e)} \sum_{\substack{\mathbf{i} \\ i_2 \neq 0}} \mathbf{u}_{1,i}^k \begin{pmatrix} \lambda_{i_1}^{1,k} \otimes \lambda_{\perp,i_2}^k \\ 0 \end{pmatrix} \\ &\quad + \sum_{i=0}^{n_- - 1} \mathbf{u}_{1,(i,0)}^- \begin{pmatrix} \lambda_i^{1,-} \otimes \bar{\lambda}_{\perp}^e \\ 0 \end{pmatrix} + \sum_{i=0}^{n_+ - 1} \mathbf{u}_{1,(i,0)}^+ \begin{pmatrix} \lambda_i^{1,+} \otimes \bar{\lambda}_{\perp}^e \\ 0 \end{pmatrix} \\ &\quad + \sum_{i=0}^{n_- - 1} \mathbf{u}_{1,(i,0)}^- \begin{pmatrix} \lambda_i^{1,-} \otimes \mathbf{c}^e \\ 0 \end{pmatrix} - \sum_{i=0}^{n_+ - 1} \mathbf{u}_{1,(i,0)}^+ \begin{pmatrix} \lambda_i^{1,+} \otimes \mathbf{c}^e \\ 0 \end{pmatrix} \\ &= \begin{pmatrix} 0 \\ \hat{u}_2 \end{pmatrix} + \sum_{k \in \mathcal{K}(e)} \sum_{\substack{\mathbf{i} \\ i_2 \neq 0}} \mathbf{u}_{1,i}^k \begin{pmatrix} \lambda_{i_1}^{1,k} \otimes \lambda_{\perp,i_2}^k \\ 0 \end{pmatrix} + \sum_{i=0}^{n_k - 1} \mathbf{u}_{1,i}^k \mathbf{u}_{1,(i,0)}^k \begin{pmatrix} \lambda_i^{1,k} \otimes \lambda_{\perp,0}^k \\ 0 \end{pmatrix} \\ &= \hat{\mathbf{u}}, \end{aligned}$$

where we used the relations (4.6) and (4.7) similar to the proof of Proposition 3.2.

- (3) The preservation of polynomial moments for \mathbf{P}_e^1 follows from that of \hat{P}_e^1 in Definition 4.3: the latter follows from the fact that \mathcal{R}^1 in Section 4.1 preserves moments of order p , and the patch-wise correction term \mathbf{C}^e guarantee the moment preservation of order r by the same arguments as for Proposition 3.2.
- (4) The edge-based operators for different edges are commuting since there are no basis functions with support on two different edges along the same axis, so we can argue as in the V^0 case: the projection \mathbf{P}_e^1 is local to the edge e and thus commutes with other local projections.

□

5. NUMERICAL EXPERIMENTS

In this Section, we verify the accuracy and well-posedness of numerical schemes using our just derived conforming projection operators, implemented in the IGA library `psydac` [25]. Based on the numerical test-cases in Section 2.6, we compare our non-matching multipatch discretization to the matching broken-FEEC framework in [26, Section 5].

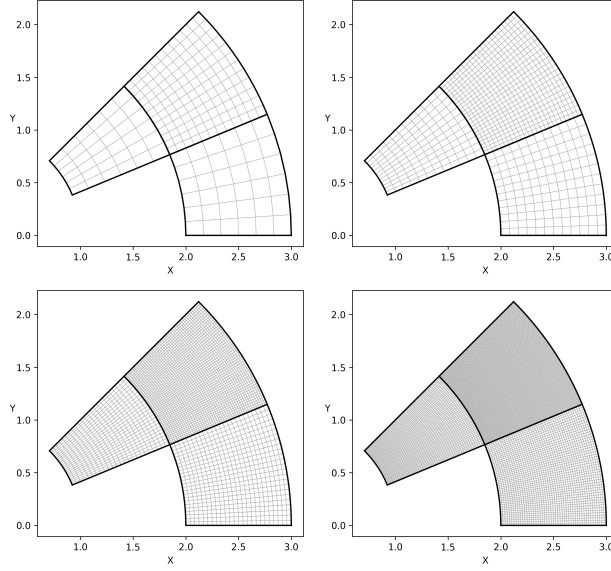


FIGURE 2. Different refinements of the curved L-shaped domain.

5.1. Approximation of the weak divergence. We apply the weak differential operators from Theorem 2.4, with their matrix form described in Section 2.6.2, to a smooth manufactured function without boundary conditions:

$$\mathbf{u}(x, y) = \begin{pmatrix} \cos(\pi x) \sin(\pi y) \\ \sin(\pi x) \cos(\pi y) \end{pmatrix} \notin H_0(\text{div}),$$

and compute the relative L^2 -error $\|\text{div}_{\text{pw}} \tilde{\Pi}_{\text{pw}}^1 \mathbf{u} - \text{div} \mathbf{u}\|_{L^2}$ for different polynomial degrees and refinement levels on a curved L-shaped domain. The different refinements are shown in Figure 2, where the corner patch is of a resolution twice as fine as the other two patches. In Figure 3, we show the convergence curve for the weak divergence operators, which coincide with the high-order approximation stated in Section 2.5.

Similarly, we can define a manufactured function for the weak **curl** operator on the same domain:

$$f(x, y) = \cos(\pi x) \cos(\pi y) \notin H_0(\mathbf{curl}),$$

and compute the relative L^2 -error $\|\mathbf{curl}_{\text{pw}} \tilde{\Pi}_{\text{pw}}^0 f - \mathbf{curl} f\|_{L^2}$. In Figure 4, we show the convergence curves for the weak **curl** operator. We observe the expected convergence behavior if polynomial moments, up to polynomial degree of the space,

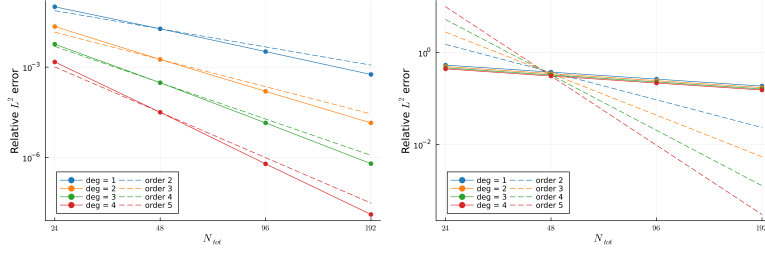


FIGURE 3. Convergence curves for the weak divergence test-case with moment preservation of order $p+1$ (left) and without (right). We plot the relative L^2 -error of the weak divergence operator for different polynomial degrees and refinement levels on the curved L-shaped domains in Figure 2.

are preserved by the operators, this breaks down if no moment preservation is applied.

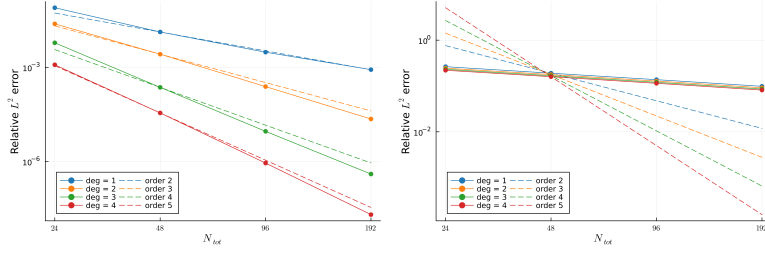


FIGURE 4. Convergence curves for the weak **curl** test-case with moment preservation of order $p+1$ (left) and without (right). We plot the relative L^2 -error of the weak **curl** operator for different polynomial degrees and refinement levels on the curved L-shaped domains in Figure 2.

5.2. Poisson problem. For this test case described in Section 2.6.3, we use the same solution (and source) as in [26, Section 5.1]. Since both are local to the upper-right handle of a pretzel shaped domain, we apply a refinement strategy that is local to this handle, which can be seen in Figure 5.

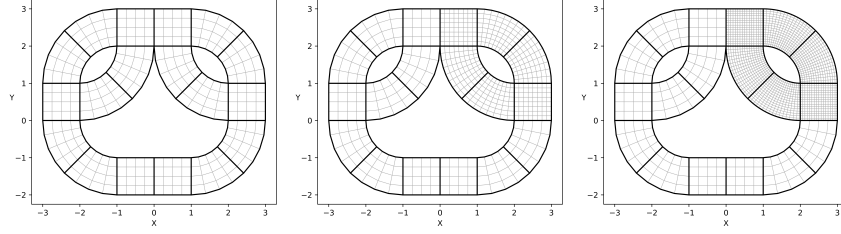


FIGURE 5. The non-matching refinements of the top-right handle of the pretzel domain.

The numerical solutions, which also virtually vanish outside this top-right handle, are shown in Figure 6.

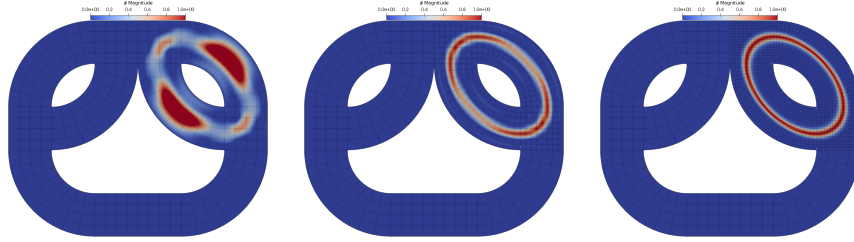


FIGURE 6. The numerical solutions of the Poisson problem for spline degree 3 on the domains from Figure 5.

In Table 1, we compare the relative L^2 -errors of manufactured solution of different polynomial degrees and number of cells per patch in the matching- and non-matching case. We observe that we achieve the same accuracy in the non-matching and the matching case, while requiring significantly fewer degrees of freedom.

Cells p.p. \ Degree	uniform refinement				refined handle	
	3	4	5	3	4	5
4×4	0.8652	0.3446	0.1831	0.8652	0.3446	0.1831
8×8	0.0460	0.0867	0.0556	0.0460	0.0867	0.0557
16×16	0.0048	0.0057	0.0036	0.0048	0.0057	0.0036

TABLE 1. Relative L^2 -errors for the Poisson problem, where the cells per patch are uniform in the matching case and as in Figure 5 for the refined handle case.

5.3. Time-harmonic Maxwell problem. We described this problem in Section 2.6.4 and, again, use the manufactured solution and source from [26, Section 5.4], which are products of sine and cosine terms on the full pretzel domain without boundary conditions. In the non-matching case, we refine every other patch by a factor of two, as shown in Figure 7, to obtain a first comparison of the convergence curves with the matching discretization.

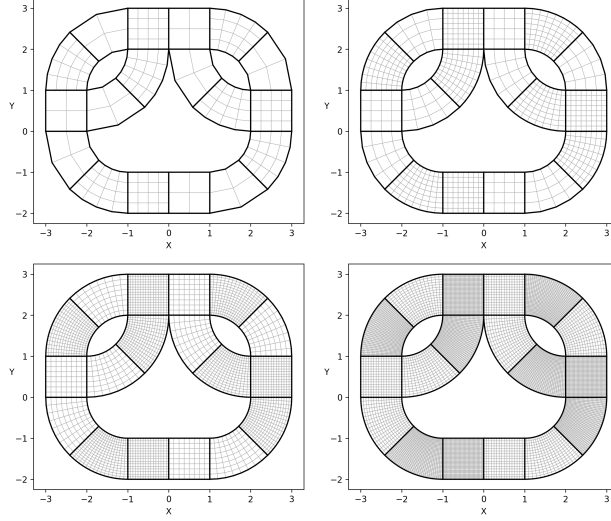


FIGURE 7. Refined grids of a pretzel shaped domain by a factor of two on every other patch.

In Figure 8, we show the convergence rates for both cases which match with the theory. Additionally, we show the magnitude of the numerical solution on a non-matching grid in Figure 8.

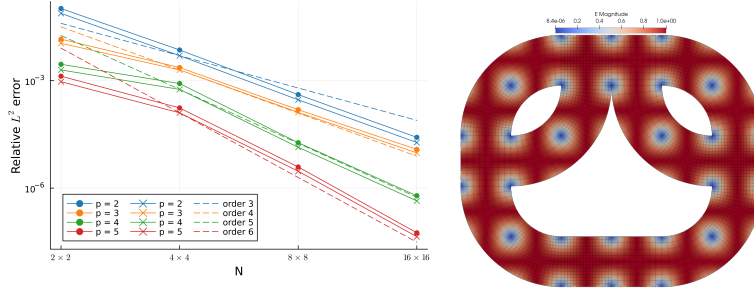


FIGURE 8. On the left, we plot the convergence curves for uniform (circle) and refined (cross) grids from Figure 7, where the abscissa describes the coarsest number of cells across all patches. On the right, we show the amplitude of the numerical solution \mathbf{E}_h for spline degree $p = 3$ on the refined domain in the bottom-left of Figure 7.

5.4. curl-curl eigenvalue problem. We refine the curved L-shaped domain with layers of finer patches around the reentrant corner, which can be seen in Figure 9.

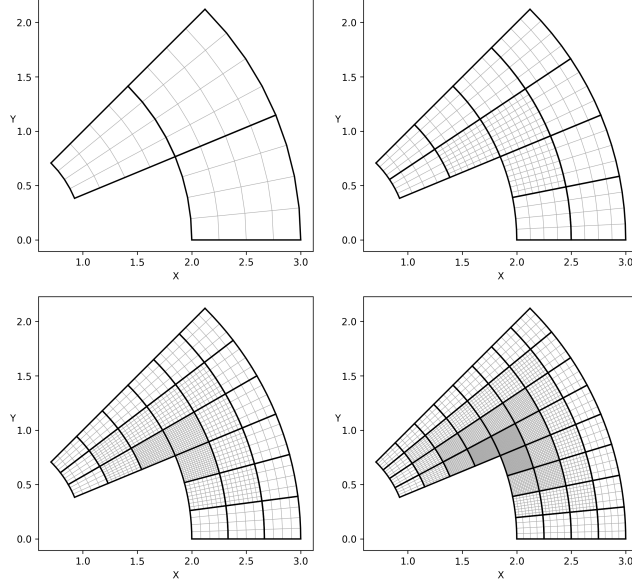


FIGURE 9. Grid refinement of the reentrant corner by adding patches of higher resolution.

Solving the **curl-curl** eigenvalue problem from Section 2.6.5 on this domain, we obtain the first five eigenvalues and compare them to a matching discretization with a comparable number of degrees of freedom.

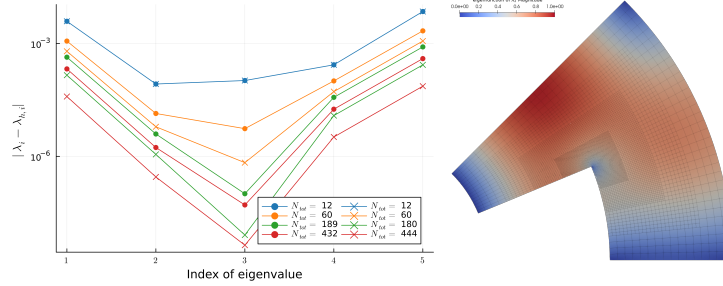


FIGURE 10. On the left, we plot the error of the first five eigenvalues for matching (circle) and non-matching (cross) domains computed with spline spaces of degree $p = 3$. We use the refinement strategy of Figure 9 and compare the results to a matching discretization with a comparable number of DOF. On the right, we show the absolute value of the eigenfunction corresponding to the second eigenvalue λ_2 on the most refined grid.

The results can be seen in Figure 10, where we plot the error for each eigenvalue for both discretizations to show spectral correctness and the benefit of refining the

reentrant corner, leading to a better approximation of the eigenfunctions. Additionally, in Figure 10, we show the absolute value of the eigenfunction corresponding to the second eigenvalue, which has a singularity at the corner.

In [18], where we showed the existence of bounded commuting projections for these non-matching multipatch domains, we had limitations when it comes to certain grid configurations or refinements. For example, the theory does yet not cover the case of three-patch domains, but we did not observe any issues in our numerical experiments. In particular in Figure 11, we present the spectral correctness of the **curl-curl** eigenvalue problem on a three-patch domain.

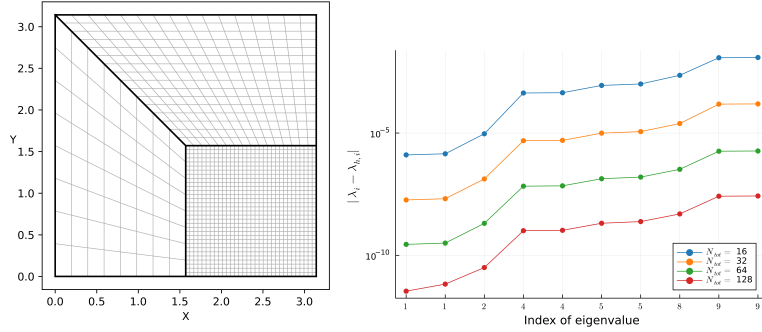


FIGURE 11. The **curl-curl** eigenvalue problem on a three-patch domain, shown left, and the error of the first ten eigenvalues on the right.

5.5. Time-domain Maxwell. We finally consider the approximation of Maxwell's equations from Section 2.6.6 on a square domain $\Omega = [0, \pi] \times [0, \pi]$ without any boundary conditions. As an initial condition, we set:

$$\mathbf{E}(t=0, \mathbf{x}) = \frac{1}{\sigma^2} \begin{pmatrix} x_2 - \bar{x}_2 \\ -(x_1 - \bar{x}_1) \end{pmatrix} e^{-\frac{\|\mathbf{x} - \bar{\mathbf{x}}\|_2^2}{2\sigma^2}}, \quad \mathbf{B}(t=0, \mathbf{x}) = \text{curl } \mathbf{E}, \quad \mathbf{J}(t, \mathbf{x}) = 0,$$

where $\bar{\mathbf{x}} = (0.5\pi, 0.5\pi)$ and $\sigma = 0.1$. As a time discretization, we cast our semi-discretization (2.21) into a simple leap-frog time-stepping scheme for some time-step $\Delta t > 0$, which reads

$$\begin{aligned} \mathbf{b}^{n+\frac{1}{2}} &= \mathbf{b}^n - \frac{\Delta t}{2} \mathbf{C} \mathbf{P}^1 \mathbf{e}^n, \\ \mathbf{M}^1 \mathbf{e}^{n+1} &= \mathbf{M}^1 \mathbf{e}^n + \Delta t (\mathbf{C} \mathbf{P}^1)^T \mathbf{M}^2 \mathbf{b}^{n+\frac{1}{2}}, \\ \mathbf{b}^{n+1} &= \mathbf{b}^{n+\frac{1}{2}} - \frac{\Delta t}{2} \mathbf{C} \mathbf{P}^1 \mathbf{e}^{n+1}. \end{aligned}$$

For our test-cases, we consider two different patch configurations: a coarse patch enclosed with fine patches and a fine patch enclosed with coarse patches as is shown in the left column of Figure 12.

We use spline spaces of degree $p = 3$ and set the order of preservation of polynomial moments $r = p + 1$ to the spline degree. Observing the discrete solution over time, we see that as the Gaussian pulse leaves the interior patch, we get spurious reflections if the conforming projection operators do not preserve polynomial moments, as shown in Figure 12. These reflections are significantly reduced

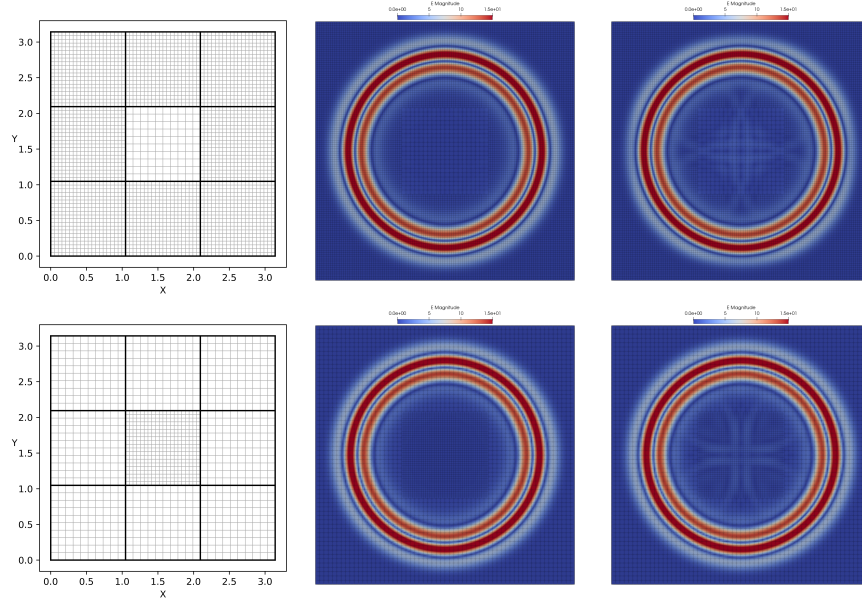


FIGURE 12. The grid setup (left) and the amplitude of the electric field \mathbf{E}_h of the time-domain Maxwell problem after leaving the interior patch. Where the discretization in the middle involves a conforming projection that preserves polynomial moments up to the polynomial degree, while the discretization on the right does not.

and virtually vanishing if the conforming projection operators preserve polynomial moments. As we experimented with many grid configurations, this is a common behavior we observed, when an edge is shared by patches of different resolution.

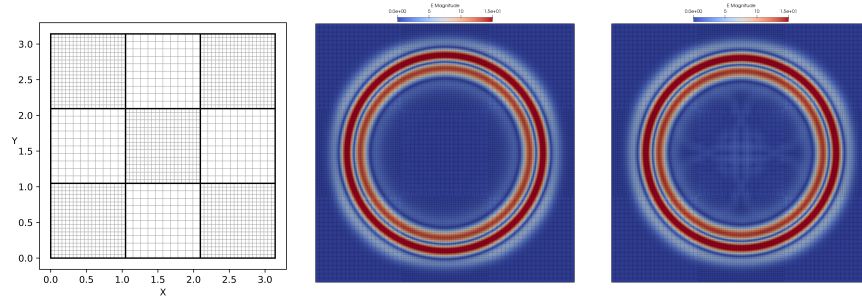


FIGURE 13. The checkerboard grid setup (left) and the amplitude of the electric field \mathbf{E}_h of the time-domain Maxwell problem after leaving the interior patch. Where the discretization in the middle involves a conforming projection that preserves polynomial moments up to the polynomial degree, while the discretization on the right does not.

Another grid setup that falls beyond the a priori stability analysis of [18], is the case of refinements in a checkerboard pattern. In Figure 13, we show the electric field of the time-domain Maxwell problem on a grid with a checkerboard refinement pattern, which has the same behavior as the two grid setups before.

5.6. Time-domain Helmholtz. For the time-domain Helmholtz problem from Section 2.6.7 with the same configuration as above, we obtain a similar leap frog time-stepping scheme, which reads

$$\begin{aligned}\mathbf{u}^{n+\frac{1}{2}} &= \mathbf{u}^n - \frac{\Delta t}{2} \mathbf{GP}^0 \phi^n, \\ \mathbf{M}^0 \phi^{n+1} &= \mathbf{M}^0 \phi^n + \Delta t (\mathbf{GP}^0)^T \mathbf{M}^1 \mathbf{u}^{n+\frac{1}{2}}, \\ \mathbf{u}^{n+1} &= \mathbf{u}^{n+\frac{1}{2}} - \frac{\Delta t}{2} \mathbf{GP}^0 \phi^{n+1}.\end{aligned}$$

The main difference is that this case involves the $\ell = 0$ conforming projection P^0 , in contrast to the P^1 projection in the Maxwell case. To verify this test-case, we used a similar setup as for the time-domain Maxwell problem, which showed the same behavior as before, i.e. we see a good reduction of spurious reflections when employing preservation of polynomial moments in the conforming projection operator.

6. CONCLUSION

In this work, we have extended the broken-FEEC approach of [26] to non-matching interfaces, which allows for a more flexible (through local refinements) and efficient treatment of multipatch spaces. This is made possible by the construction of conforming projection operators for the non-conforming multipatch spaces V^0 and V^1 , where we put special emphasis on the preservation of polynomial moments.

In conclusion, we showed the practicability and efficiency of broken-FEEC algorithms using our novel conforming projection operators in the numerical treatment of different PDE problems. In particular, thanks to the preservation of polynomial moments, we were able to reduce spurious reflections/oscillations in the context of electromagnetic wave equations.

REFERENCES

1. Douglas N. Arnold, Pavel B. Bochev, Richard B. Lehoucq, Roy A. Nicolaides, and Mikhail Shashkov (eds.), *Compatible spatial discretizations*, The IMA Volumes in Mathematics and its Applications, vol. 142, Springer, New York, 2006. MR 2256572
2. Douglas N. Arnold, Richard S. Falk, and Ragnar Winther, *Finite element exterior calculus, homological techniques, and applications*, Acta Numerica **15** (2006), 1–155 (English).
3. ———, *Finite element exterior calculus: From Hodge theory to numerical stability*, Bull. Am. Math. Soc., New Ser. **47** (2010), no. 2, 281–354 (English).
4. Pavel B. Bochev and James M. Hyman, *Principles of Mimetic Discretizations of Differential Operators*, Compatible Spatial Discretizations (New York, NY) (Douglas N. Arnold, Pavel B. Bochev, Richard B. Lehoucq, Roy A. Nicolaides, and Mikhail Shashkov, eds.), The IMA Volumes in Mathematics and its Applications, Springer, 2006, pp. 89–119 (en).
5. Daniele Boffi, *Compatible Discretizations for Eigenvalue Problems*, Compatible Spatial Discretizations, Springer New York, New York, NY, 2006, pp. 121–142.
6. Daniele Boffi, Franco Brezzi, and M Fortin, *Mixed finite element methods and applications*, Springer Series in Computational Mathematics, vol. 44, Springer, 2013.

7. Daniele Boffi, Martin Costabel, Monique Dauge, Leszek Demkowicz, and Ralf Hiptmair, *Discrete compactness for the p -version of discrete differential forms*, SIAM Journal on Numerical Analysis **49** (2011), no. 1, 135–158.
8. Alain Bossavit, *Whitney forms: a class of finite elements for three-dimensional computations in electromagnetism*, Physical Science, Measurement and Instrumentation, Management and Education - Reviews, IEE Proceedings A, vol. 135, 1988, pp. 493 – 500.
9. ———, *Computational electromagnetism. Variational formulations, complementarity, edge elements*, Orlando, FL: Academic Press, 1998 (English).
10. Annalisa Buffa, Jürgen Dölz, Stefan Kurz, Sebastian Schöps, Rafael Vázquez, and Felix Wolf, *Multipatch approximation of the de Rham sequence and its traces in isogeometric analysis*, Numerische Mathematik **144** (2019), no. 1, 201 – 236.
11. Annalisa Buffa and Ilaria Perugia, *Discontinuous Galerkin Approximation of the Maxwell Eigenproblem*, SIAM Journal on Numerical Analysis **44** (2006), no. 5, 2198–2226.
12. Annalisa Buffa, Ilaria. Perugia, and Tim Warburton, *The Mortar-Discontinuous Galerkin Method for the 2D Maxwell Eigenproblem - Springer*, Journal of Scientific Computing (2009).
13. Annalisa Buffa, Judith Rivas, Giancarlo Sangalli, and Rafael Vázquez, *Isogeometric Discrete Differential Forms in Three Dimensions*, SIAM Journal on Numerical Analysis **49** (2011), no. 2, 818–844, Publisher: Society for Industrial and Applied Mathematics.
14. Annalisa Buffa, Giancarlo Sangalli, and Rafael Vázquez, *Isogeometric analysis in electromagnetics: B-splines approximation*, Computer Methods in Applied Mechanics and Engineering **199** (2010), no. 17, 1143–1152 (en).
15. ———, *Isogeometric methods for computational electromagnetics: B-spline and T-spline discretizations*, Journal of Computational Physics **257** (2014), 1291–1320 (en).
16. Annalisa Buffa, Rafael Vázquez, Giancarlo Sangalli, and Lourenço Beirão da Veiga, *Approximation estimates for isogeometric spaces in multipatch geometries*, Numerical Methods for Partial Differential Equations **31** (2015), no. 2, 422 – 438 (English).
17. Martin Campos Pinto and Yaman Güçlü, *Broken-FEEC discretizations and Hodge Laplace problems*, Mathematics of Computation (2025) (English).
18. Martin Campos Pinto and Frederik Schnack, *Bounded commuting projections for multipatch spaces with non-matching interfaces*, The SMAI Journal of computational mathematics **11** (2025), 85–137 (en).
19. Martin Campos Pinto and Eric Sonnendrücker, *Gauss-compatible Galerkin schemes for time-dependent Maxwell equations*, Math. Comput. **85** (2016), no. 302, 2651–2685 (English).
20. Sven Chilton, *A fourth-order adaptive mesh refinement solver for Maxwell’s Equations*, Ph.D. thesis, University of California, Berkeley, January 2013.
21. Sven H. Chilton and Phillip Colella, *Damping of spurious wave reflections from coarse-fine adaptive mesh refinement grid boundaries*, 2010 Abstracts IEEE International Conference on Plasma Science, 2010.
22. John A Evans, Michael A Scott, Kendrick M Shepherd, Derek C Thomas, and Rafael Vázquez, *Hierarchical B-spline complexes of discrete differential forms*, IMA Journal of Numerical Analysis **40** (2020), no. 1, 422–473 (en).
23. Jason Frank and Sebastian Reich, *On spurious reflections, nonuniform grids and finite difference discretizations of wave equations*, Modelling, Analysis and Simulation Report MAS-E0406, Stichting Centrum voor Wiskunde en Informatica, May 2004.
24. Vivette Girault and Pierre-Arnaud Raviart, *Finite Element Methods for Navier-Stokes Equations – Theory and Algorithms*, Springer Series in Computational Mathematics, Springer-Verlag, Berlin, 1986.
25. Y. Güçlü, S. Hadjout, and A. Ratnani, *Psydac: a high-performance iga library in python*, 8th European Congress on Computational Methods in Applied Sciences and Engineering, ECCOMAS Congress 2022, CIMNE, 2022.
26. Yaman Güçlü, Said Hadjout, and Martin Campos Pinto, *A Broken FEEC Framework for Electromagnetic Problems on Mapped Multipatch Domains*, Journal of Scientific Computing **97** (2023), no. 2, 52 (en).
27. R. Hiptmair, *Canonical construction of finite elements*, Mathematics of Computation **68** (1999), no. 228, 1325–1346.
28. Ralf Hiptmair, *Finite elements in computational electromagnetism*, Acta Numerica **11** (2002), 237–339.

29. Florian Holderied, Stefan Possanner, and Xin Wang, *MHD-kinetic hybrid code based on structure-preserving finite elements with particles-in-cell*, Journal of Computational Physics **433** (2021), 110143.
30. Thomas J R Hughes, J A Cottrell, and Y Bazilevs, *Isogeometric analysis: CAD, finite elements, NURBS, exact geometry and mesh refinement*, Computer Methods in Applied Mechanics and Engineering **194** (2005-10), no. 39-41, 4135 – 4195 (English).
31. Kjetil André Johannessen, Mukesh Kumar, and Trond Kvamsdal, *Divergence-conforming discretization for Stokes problem on locally refined meshes using LR B-splines*, Computer Methods in Applied Mechanics and Engineering **293** (2015), 38–70 (en).
32. Jasper Kreeft, Artur Palha, and Marc Gerritsma, *Mimetic framework on curvilinear quadrilaterals of arbitrary order*, 2011.
33. J.-C. Nédélec, *Mixed finite elements in \mathbf{R}^3* , Numerische Mathematik **35** (1980), no. 3, 315–341.
34. Francesco Patrizi, *Isogeometric de Rham complex discretization in solid toroidal domains*, June 2021, arXiv:2106.10470 [cs, math].
35. Les Piegl and Wayne Tiller, *The NURBS book*, Monographs in Visual Communication, Springer, Berlin, Germany, July 2012 (en).
36. P.-A. Raviart and J.-M. Thomas, *A mixed finite element method for 2nd order elliptic problems*, Mathematical aspects of finite element methods, Lecture Notes in Math., Vol. 606, Springer, Berlin, 1977, pp. 292–315.
37. Larry Schumaker, *Spline functions: basic theory*, third ed., Cambridge University Press, Cambridge University Press, 2007.
38. Deepesh Toshniwal and Thomas J. R. Hughes, *Isogeometric discrete differential forms: Non-uniform degrees, Bézier extraction, polar splines and flows on surfaces*, Computer Methods in Applied Mechanics and Engineering **376** (2021), 113576 (en).
39. J.-L. Vay, J.-C. Adam, and A. Héron, *Asymmetric pml for the absorption of waves. application to mesh refinement in electromagnetic particle-in-cell plasma simulations*, Computer Physics Communications **164** (2004), no. 1, 171–177, Proceedings of the 18th International Conference on the Numerical Simulation of Plasmas.

APPENDIX A. HOMOGENEOUS BOUNDARY CONDITIONS

In order to use our scheme for sequences with homogeneous boundary conditions, we can extend our construction. This boils down to do modifying the edge- and vertex conforming projections for edges and vertices that lie on the domain boundary.

First, we look at the V^0 case discussed in Section 3 and extend Definition 3.5 to vertices on the boundary: Let $v \in \mathcal{V}$ be a boundary vertex, then

$$P_v : \Lambda_j^k \mapsto \begin{cases} \sum_{m_1=1}^r \sum_{m_2=1}^r \gamma_m \Lambda_m^k & \text{if } j = \mathbf{0} \text{ and } k \in \mathcal{K}(v), \end{cases}$$

where the point-value at the vertex is projected to zero, but we still have to account for the preservation of polynomial moments by interior basis functions close to the vertex.

Continuing with the edge-based projections, we similarly extend Definition 3.8 to edges on the boundary: Let k be the patch adjacent to the boundary edge e

$$P_e : \Lambda_j^k \mapsto \begin{cases} \mathcal{F}^0 \left(\sum_{m=1}^r \gamma_m^{1d} \lambda_{j_1}^k \otimes \lambda_m^k \right) & \text{if } 0 \leq j_1 \leq n_k, j_2 = 0, \\ \mathcal{F}^0 \left(\sum_{m=1}^r \gamma_m^{1d} \mu_v^- \otimes \lambda_m^k \right) & \text{if } j_1 \in \{0, n_-\}, j_2 = 0 \\ & \text{for } v \text{ at } \mathbf{j} \text{ and } v \text{ shared by another patch,} \\ \mathcal{F}^0 \left(\sum_{m_1=1}^r \sum_{m_2=1}^r \gamma_{\mathbf{m}} \Lambda_{\mathbf{m}}^k \right) & \text{if } \mathbf{j} = \mathbf{0} \text{ for } v \text{ at } \mathbf{j} \text{ and } v \text{ is only on patch } k, \end{cases}$$

where patch k adjacent to the edge e is treated as the coarse patch. Again, we project all point-values on the boundary to zero, but have to account for moment-preservation similarly to before.

This extension directly applies to the V^1 case from Section 4. The edge-conforming projection in Definition 4.3 for a boundary edge e in this case reads:

$$\hat{P}_e^1 : (\hat{\Lambda}_{1,\mathbf{j}}^{1,-})_1 \mapsto \sum_{m=1}^r \gamma_m^{1d} \lambda_{j_1}^{1,k} \otimes \lambda_m^k \quad \text{if } j_2 = 0,$$

with arguments similar to above.

APPENDIX B. IMPLEMENTATION OF CONFORMING PROJECTIONS IN PRACTICE

B.1. Correction coefficients γ . As we discussed in Remark 3.4, we can solve the linear system for the correction coefficients \mathbf{a} and $\tilde{\mathbf{a}}$ from Ansatz (3.4) independent of the patch. Similar to Section 3.1, we define the basis-polynomial duality-matrices and vertex-basis-polynomial vectors as

$$\mathbf{M} = \left(\int_0^1 \lambda_m q_j \right)_{1 \leq m \leq r, 1 \leq j \leq r}, \quad \mathbf{b} = \left(\int_0^1 \lambda_0 q_j \right)_{1 \leq j \leq r},$$

where we assume the same discretization along both axis. For the polynomial basis on the interval $[0, 1]$, we use Bernstein polynomials

$$q_j(\hat{x}) = \binom{r}{j} \hat{x}^j (1 - \hat{x})^{r-j}, \quad j = 1, \dots, r,$$

since the resulting duality-matrices have a good condition number in practice. Thus, we define the one-dimensional correction coefficient

$$\gamma^{1d} = \mathbf{M}^{-1} \mathbf{b}.$$

B.2. Matrix form of the extension- and restriction operators for V_{pw}^0 . Since both spaces have the same degree and are nested, we use the knot insertion technique for B-splines, explained for example in [35, Section 5.2], to describe the extension operator \mathcal{E}^0 from (3.10) as the matrix $\mathbf{E}^0 \in \mathbb{R}^{n_+ \times n_-}$ acting on the degrees of freedom/coefficients in these basis representations, i.e.

$$\lambda_i^- = \sum_{j=0}^{n_+} \mathbf{E}_{j,i}^0 \lambda_j^+,$$

for $i = 0, \dots, n_-$, where n_- and n_+ are the number of basis functions in the coarse and fine space, respectively. This form of the extension operator is very helpful

when it comes to implementation, as we can directly apply it to the coefficients of the coarse space.

The restriction operator \mathcal{R} in (3.11) consists of

- The interior restriction operator $\tilde{\mathcal{R}}$ is defined by the L^2 -projection in (3.15). We introduce the interior (mixed) mass-matrices

$$\begin{aligned}\tilde{\mathbf{M}}_{i,j}^{-,+} &= (\langle \lambda_i^-, \lambda_j^+ \rangle)_{i,j}, \quad i = 0, \dots, n_-, \quad j = 1, \dots, n_+ - 1, \\ \mathbf{M}_{i,j}^{-,-} &= (\langle \lambda_i^-, \lambda_j^- \rangle)_{i,j}, \quad i = 0, \dots, n_-, \quad j = 0, \dots, n_+, \end{aligned}$$

such that we can write the projection in matrix form as

$$\tilde{\mathbf{R}} = (\mathbf{M}^{-,-})^{-1} \tilde{\mathbf{M}}^{-,+}.$$

It is fully moment preserving by definition of the L^2 -projection.

- The coarse truncation $\tilde{\mathcal{T}}$ in (3.16), which we can write in matrix form $\tilde{\mathbf{T}} \in \mathbb{R}^{n_- - 2 \times n_-}$ as

$$\tilde{\mathbf{T}}_{i,j} = \begin{cases} 0 & \text{for } i = 0, n_-, \forall j, \\ 1 & \text{for } 0 < i, j < n_-, j = i, \\ \gamma_i^{1d} & \text{for } 0 < i < r+1, j = 0, \\ \gamma_{n_- - i}^{1d} & \text{for } n_- - r - 1 < i < n_-, j = n_-, \\ 0 & \text{else.} \end{cases}$$

The motivation for this matrix is given by looking at $\phi^- \in \mathbb{V}_{\parallel}^{0,-}$ and mapping $\tilde{\mathcal{T}}\phi^- = \tilde{\phi}^- \in \mathbb{V}_{\parallel,0}^{0,-}$ such that $(\tilde{\phi}^-)_0 = (\tilde{\phi}^-)_{n_-} = 0$, while preserving polynomial moments:

$$\int \tilde{\phi}^- q = \int \left(\sum_{0 < j < n_-} \phi_j^- \lambda_j^- + \sum_{0 < i < r+1} \gamma_i^{1d} \phi_0^- \lambda_i^- + \sum_{n_- - r - 1 < i < n_-} \gamma_i^{1d} \phi_{n_-}^- \lambda_i^- \right) q = \int \phi^- q,$$

by the definition of γ^{1d} in (3.7).

- The truncation \mathcal{T} in (3.14) in matrix form $\mathbf{T} \in \mathbb{R}^{n_+ - 2 \times n_+}$ can be written as

$$(\mathbf{T})_{i,j} = \begin{cases} 1 & \text{for } j = i, 1 \leq i \leq n_+ - 1 \\ -\mathbf{E}_{0,i} & \text{for } j = 0, 1 \leq i \leq n_+ - 1, \\ -\mathbf{E}_{n_+,i} & \text{for } j = n_+, 1 \leq i \leq n_+ - 1, \\ 0 & \text{else.} \end{cases}$$

This leads to the matrix form of the moment-preserving interior restriction operator in (3.17) as

$$\mathbf{R}_0 = \tilde{\mathbf{T}} \tilde{\mathbf{R}} \in \mathbb{R}^{n_+ - 2 \times n_- - 2}.$$

And in total, we can write the full restriction matrix \mathbf{R} as

$$\mathbf{R} = \begin{pmatrix} 1 & 0 & \cdots & 0 \\ \mathbf{R}_0 \mathbf{T} & & & \\ 0 & \cdots & 0 & 1 \end{pmatrix} \in \mathbb{R}^{n_- \times n_+}$$

Remark B.1. Instead of using an L^2 -projection for the restriction operator $\tilde{\mathcal{R}}$, we could, for practicability, also use a more local projection.

B.3. Matrix form of the extension- and restriction operators for V_{pw}^1 . Similarly to the V^0 case, since the nestedness still holds for the derived spaces, we can define the extension operator \mathcal{E}^1 from (4.3) as the matrix $\mathbf{E}^1 \in \mathbb{R}^{n_+-1 \times n_- - 1}$ defined by knot insertion from [35, Section 5.2].

The restriction operator \mathcal{R}^1 from (4.4) is now purely defined as the L^2 -projection (4.5) and thus can be written as the matrix

$$\mathbf{R}^1 = (\mathbf{M}^{1,-,-})^{-1} \mathbf{M}^{1,-,+} \in \mathbb{R}^{n_- - 1 \times n_+ - 1},$$

with the mass matrices

$$\mathbf{M}_{i,j}^{1,\pm,\pm} = \left(\langle \lambda_i^{1,\pm}, \lambda_j^{1,\pm} \rangle \right)_{i,j}, \quad i = 0, \dots, n_{\pm} - 1, \quad j = 0, \dots, n_{\pm} - 1.$$

This restriction operator is already moment-preserving by definition and needs no further modifications.

MAX-PLANCK-INSTITUT FÜR PLASMAPHYSIK, BOLTZMANNSTR. 2, 85748 GARCHING, GERMANY

Email address: frederik.schnack@ipp.mpg.de

MAX-PLANCK-INSTITUT FÜR PLASMAPHYSIK, BOLTZMANNSTR. 2, 85748 GARCHING, GERMANY

Email address: martin.campos-pinto@ipp.mpg.de